Nonlinear Dyn (2007) 49:375–399
DOI 10.1007/s11071-006-9129-6

ORIGINAL ARTICLE

Order reduction of structural dynamic systems with static piecewise linear nonlinearities

Eric A. Butcher · Rongdong Lu

Received: 6 September 2002 / Accepted: 24 November 2004 / Published online: 5 January 2007

Abstract A technique for order reduction of dynamic systems in structural form with static piecewise linear nonlinearities is presented. By utilizing two methods which approximate the nonlinear normal mode (NNM) frequencies and mode shapes, reduced-order models are constructed which more accurately represent the dynamics of the full model than do reduced models obtained via standard linear transformations. One method builds a reduced-order model which is dependent on the amplitude (initial conditions) while the other method results in an amplitude-independent reduced model. The two techniques are first applied to reduce two-degree-of-freedom undamped systems with clearance, deadzone, bang-bang, and saturation stiffness nonlinearities to single-mode reduced models which are compared by direct numerical simulation with the full models. It is then shown via a damped four-degree-of-freedom system with two deadzone nonlinearities that one of the proposed techniques allows for reduction to multi-mode reduced models and can accommodate multiple nonsmooth static nonlinearities with several surfaces of discontinuity. The advantages of the proposed methods include obtaining a reduced-order model which is signal-independent (doesn't require direct integration of the full model), uses a subset of the original physical coordinates, retains the form of the nonsmooth nonlinearities, and closely tracks the actual NNMs of the full model.

Keywords Piecewise linear nonlinearities · Order reduction · Nonlinear normal modes

E. A. Butcher (✉) · R. Lu
Department of Mechanical Engineering, University of Alaska Fairbanks, Fairbanks, AK 99775-5905, USA
e-mail: ffeab@uaf.edu

1 Introduction

Nonsmooth nonlinearities exist in many mechanical systems either by design or as the result of wear or failure. In particular, systems with piecewise linear static nonlinearities include bilinear and trilinear systems with clearance, deadzone, bang-bang, and saturation nonlinearities. These systems are of great importance in the modeling of such phenomena as joint dynamics [1], turbines and compressors subjected to casing rub [2], rotor-bearing systems with deadzone [3], and transmission gears with backlash [4]. Accurate reduced-order models of large dimensional nonsmooth systems are an invaluable aid in the analysis and control of such systems. Such reduced-order models are approximations to the actual nonlinear normal modes (NNMs) of the full model. Important contributions to the subject of NNMs in nonsmooth systems include references [5–9]. In [9] the NNM frequencies of a nonsmooth bilinear system with nonvanishing clearance were approximated using three analytical techniques which are based on the well-known bilinear frequency relation. The results were compared with those obtained from numerical simulations of the NNMs.

The subject of order reduction of nonsmooth systems has been studied very recently. Rhee and Burton [10] applied a previously developed linear-based Guyan-like reduction procedure which preserves the exact eigenstructure of the linearized model [11, 12] to the cases of deadzone and bang-bang nonlinearities in a two-degree-of-freedom vibrating system. The frequencies of the reduced models were compared with those of the actual NNMs in the full model obtained by direct numerical simulation. The method has the advantages that the coordinates of the reduced-order model are a subset of the original physical coordinates (as is preferred in structural dynamics and finite element analysis), the form of the nonsmooth nonlinearity is retained in the reduced model, and the linear transformation between master and slave coordinates is easy to apply for large-scale models. However, because the nonlinearity is not accounted for in the transformation, the frequency – amplitude dependence obtained from the reduced models differ significantly from that of the NNMs of the full model.

A more accurate method pursued in [13] involves applying a nonsmooth Galerkin-based order reduction transformation which takes the nonlinearity into account in order to obtain the invariant manifolds and their associated dynamics for each mode. This had been previously accomplished for smooth nonlinearities in [14–16]. This technique extended the earlier results for nonsmooth systems in [7] to larger amplitudes. However, the reduced model is obtained in terms of amplitude-phase coordinates of the modal form instead of the physical coordinates. In addition, large numbers of nonlinear algebraic equations must be solved (even for low-order systems) and the method is not easily applied to systems with multiple nonsmooth nonlinearities or several surfaces of discontinuity.

Here, an alternative technique is proposed for order reduction of structural dynamic systems with static piecewise linear nonlinearities in which the linear part of the model dominates in the dynamics. This is done in an effort to retain the advantages of the linear-based reduction method used in [10–12] while improving on the accuracy of the reduced model. This is accomplished by approximating the amplitude-dependent NNM frequencies and mode shapes of the full model using linear approximation methods based on extensions of the bilinear frequency relation. It is shown that when only one master coordinate is retained, the exact frequency of the reduced order model may be derived analytically and used to approximate the NNM frequency of the full model. In this context, the linear-based order reduction procedure serves as a method for approximating the true NNM frequencies as in [9]. Improved reduced-order models are then constructed which are closer approximations to the NNMs for the full model than are those obtained via the linear-based transformation. For this purpose, two approximation techniques, called the piecewise modal method (PMM) and local equivalent linear stiffness method (LELSM) in [9], are utilized. The technique is first applied to reduce two-degree-of-freedom undamped systems with clearance, deadzone, bang-bang, and saturation static nonlinearities to single-mode reduced models which are either amplitude-independent (for PMM) or amplitude-dependent (for LELSM). A damped four-degree-of-freedom system with two deadzone nonlinearities and multiple surfaces of discontinuity is then reduced to a multi-mode reduced model. In LELSM the amplitude dependence on the nonlinear coefficients in the reduced model can be obtained by specifying the total energy of the undamped system without the need for direct integration of the full model in advance. It is shown via direct simulation that the improved reduced models are much better at tracking the NNMs of the full models than those obtained via the linear-based transformation.

2 Linear-based order reduction

Consider the system of n second-order differential equations in structural form

$$M\ddot{x} + C\dot{x} + Kx + F(x) = G(t) \tag{1}$$

where the static piecewise linear nonlinearities $F(x)$ are isolated to the first m coordinates and m equations, i.e.

$$F(x) = [f_1(x_1, \ldots x_m) \ldots f_m(x_1, \ldots x_m) 0 \ldots 0]^T \tag{2}$$

where $f_i(), i = 1, \ldots, m$ are piecewise linear functions. It is desired to reduce Equation (1) to a set of m master coordinates x_1,...,x_m, eliminating the $s = n - m$ slave coordinates $x_{m+1}, \ldots, x_n$. For this purpose, the displacement vector x is partitioned into $m \times 1$ and $s \times 1$ master and slave vectors as $x = [x_m^T \;\; x_s^T]^T$. The undamped, unforced, linear part of (1) is

$$M\ddot{x} + Kx = 0 \tag{3}$$

which has eigenfrequencies ω_i and eigenvectors ϕ_i. Typically the modes with the lowest frequencies are retained in the reduced-order model.

To construct the linear-based reduced model, let the $n \times m$ transformation matrix be defined as

$$\Phi = \begin{bmatrix} I_m \\ T \end{bmatrix} \tag{4}$$

in which I_m is the $m \times m$ identity matrix and the $(n-m) \times m$ matrix T is found by iterating the following equation [11, 12]

$$\begin{aligned} T = &-[k_{ss} - (m_{ss}T + m_{sm})(m_{ms}T + m_{mm})^{-1}k_{ms}]^{-1} \\ &\times [k_{sm} - (m_{ss}T + m_{sm})(m_{ms}T + m_{mm})^{-1}k_{mm}] \end{aligned} \tag{5}$$

where the mass and stiffness matrices in Equation (3) are partitioned as

$$M = \begin{bmatrix} m_{mm} & m_{ms} \\ m_{sm} & m_{ss} \end{bmatrix} \quad K = \begin{bmatrix} k_{mm} & k_{ms} \\ k_{sm} & k_{ss} \end{bmatrix} \tag{6}$$

Applying the transformation

$$x = \Phi x_m \tag{7}$$

to Equation (1) and premultiplying by Φ^T yields

$$\tilde{M}\ddot{x}_m + \tilde{C}\dot{x}_m + \tilde{K}x_m + f(x_m) = \tilde{G}(t) \tag{8}$$

where

$$\begin{aligned} &\tilde{M} = \Phi^T M \Phi \quad \tilde{C} = \Phi^T C \Phi \quad \tilde{K} = \Phi^T K \Phi \\ &f(x_m) = [f_1(x_m) \dots f_m(x_m)]^T \quad \tilde{G}(t) = \Phi^T G(t) \end{aligned} \tag{9}$$

It should be noted that Equation (7) implies a relationship

$$x_s = T x_m \tag{10}$$

between the master and slave coordinates and that the retained coordinates are a subset of the original physical coordinates. It was shown in [11, 12] that T preserves the exact eigenstructure of Equation (3). Equation (7) is thus a Guyan-like order reduction transformation which accounts for the inertia as well as stiffness effects. When the mass terms are set to zero in Equation (5), the traditional Guyan reduction transformation $T = -k_{ss}^{-1}k_{sm}$ is produced [17].

If only one master coordinate is retained ($m = 1$), then $\Phi = \phi_i$ (the eigenvector corresponding to he retained mode normalized such that the first element is one) and Equation (7) becomes

$$x = \phi_i x_1 \tag{11}$$

If there is no damping or forcing, then the single-mode reduced model becomes

$$\ddot{x}_1 + \omega_i^2 x_1 + \beta_i f(x_1) = 0 \tag{12}$$

where

$$\omega_i = \sqrt{\frac{\phi_i^T K \phi_i}{\phi_i^T M \phi_i}} \quad \beta_i = \frac{1}{\phi_i^T M \phi_i} \tag{13}$$

are the ith modal frequency of Equation (3) and the reduced nonlinear coefficient for the ith mode. It is desirable that the dynamics of the amplitude-independent reduced model of Equation (12) are close to those of the ith NNM of the original full model. However, Rhee and Burton [10] found that the nonlinear frequencies of Equation (12) for deadzone and bang-bang nonlinearities in a two-degree-of-freedom system diverged from the NNM frequencies of the full model as the frequencies increased. This error for these cases as well as for bilinear clearance and saturation nonlinearities is shown later.

3 Approximation of NNM frequencies via linear-based reduced models

3.1 Bilinear clearance nonlinearity

Here, the linear-based reduced-order model obtained in the last section is used to obtain an estimate of the NNM frequencies. If only one master coordinate is retained in the linear-based order reduction of an undamped, unforced system with a piecewise linear stiffness, then the periodic motion of Equation (12) has a closed form expression whose exact frequency can be easily obtained. As an illustrative example, consider the

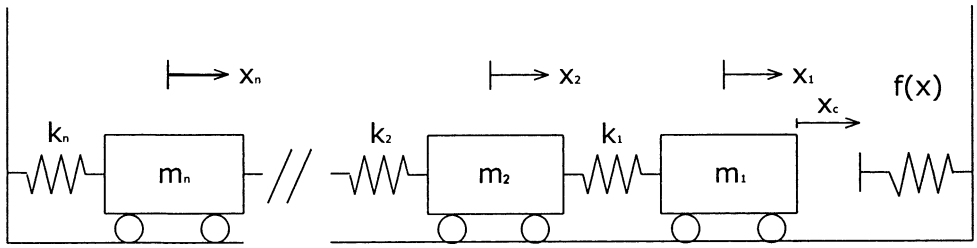

Fig. 1 An n-degree-of-freedom bilinear vibrating system with a clearance nonlinearity

n-degree-of-freedom conservative vibrating system with a nonvanishing clearance in Fig. 1 with equations of motion

$$
\begin{aligned}
&m_1\ddot{x}_1 + k_1x_1 - k_1x_2 + f(x_1) = 0\\
&m_2\ddot{x}_2 + (k_1 + k_2)x_2 - k_1x_1 + k_2x_3 = 0\\
&\cdots\\
&m_n\ddot{x}_n + (k_{n-1} + k_n)x_n - k_{n-1}x_{n-1} = 0\\
&f(x_1) = \begin{cases} 0; & x_1 < x_c \\ k_c(x_1 - x_c); & x_1 > x_c \end{cases}
\end{aligned}
\tag{14}
$$

The asymmetric bilinear stiffness of the first mass is divided into two distinct linear subregions. Since the clearance x_c is *not* restricted to be positive, a negative clearance, or interference, is also allowed. Since the masses' positions are measured from equilibrium, penetration into the second subregion is made only when the energy of the system is sufficient such that the clearance is traversed by the first mass, i.e. $x_1 > x_c$. Otherwise if the energy is insufficient for contact with the free spring, then the system remains in the first linear subregion. In the case of interference, the energy must be sufficient for the first subregion to be obtained (i.e. $x_1 < x_c$); otherwise the system remains continuously in contact with the free spring.

The scaled variables

$$
\begin{aligned}
&\kappa_c = \frac{k_c}{k_1} \quad \omega_- = \sqrt{\frac{k_1}{m_1}} \quad \omega_+ = \sqrt{\frac{k_1 + k_c}{m_1}}\\
&\alpha = \frac{\omega_+}{\omega_-} = \sqrt{1 + \kappa_c}
\end{aligned}
\tag{15}
$$

are now introduced where ω_- and ω_+ are the linear frequencies of vibration of m_1 (with m_2 held still) in the first and second linear subregions, respectively. The total period of the single-degree-of-freedom version of Equation (14)

$$
m\ddot{x}_1 + kx_1 + f(x_1) = 0
$$

$$
f(x_1) = \begin{cases} 0; & x_1 < x_c \\ k_c(x_1 - x_c); & x_1 > x_c \end{cases}
\tag{16}
$$

can be found by integrating over the closed path Γ as

$$
T = \oint_\Gamma dt = 2\int_{-x_0}^{x_c} \frac{1}{\dot{x}_-} dx_- + 2\int_{x_c}^{x_c + D_+} \frac{1}{\dot{x}_+} dx_+
\tag{17}
$$

in terms of the closed orbits in the phase plane $x_-^2 + \dot{x}_-^2 = x_0^2$ and $\alpha^2(x_+ - x_e)^2 + \dot{x}_+^2 = x_0^2 - x_c x_e$ where $x_e = (1 - 1/\alpha^2)x_c$ from which the velocities in the above integrals are determined. The amplitude is x_0 and

$$
D_+ = \frac{x_0}{\alpha}\sqrt{1 - \rho^2\left(1 - \frac{1}{\alpha^2}\right)} - \frac{x_c}{\alpha^2}
\tag{18}
$$

is the penetration distance into the second subregion [9]. The dimensionless clearance parameter $\rho = x_c/x_0$ must lie in the interval $[-1, 1]$ if the clearance boundary is crossed. Evaluation of these integrals yields the oscillation period from which the frequency is found as

$$
\begin{aligned}
\Omega = 2\omega_-\omega_+\Bigg[&\omega_+\left(1 + \frac{2}{\pi}\sin^{-1}\rho\right) + \omega_-\\
&\times\left(1 - \frac{2}{\pi}\sin^{-1}\left(\frac{\rho}{\alpha\sqrt{1 - \rho^2(1 - \frac{1}{\alpha^2})}}\right)\right)\Bigg]^{-1}
\end{aligned}
\tag{19}
$$

Note the amplitude dependence enters Equation (19) through the parameter ρ. When the clearance vanishes

($\rho = 0$) Equation (19) becomes the amplitude-independent "bilinear frequency relation"

$$\Omega = \frac{2\omega_-\omega_+}{\omega_+ + \omega_-} \tag{20}$$

which has appeared in several studies of bilinear systems with vanishing clearance, e.g. [18]. It should be noted that for the single-degree-of-freedom reduced model in Equation (12) with $f(x_1)$ given in Equation (16), the two linear frequencies are $\omega_- = \omega_i$ and $\omega_+ = \sqrt{\omega_i^2 + \beta_i k_c}$ so that $\alpha = \sqrt{\omega_i^2 + \beta_i k_c}/\omega_i$. Hence, the reduced-order model of Equation (12) provides an alternative route for estimating the BNM frequencies via Equations (19) or (20). In Fig. 2, the approximate BNM frequencies in both modes of the two-degree-of-freedom version of Equation (14) obtained from the linear-based reduced model as well as the PMM and LELSM methods (to be discussed) are plotted versus ρ for $\alpha^2 = 2$ along with the exact BNM frequencies found by direct numerical simulation of the

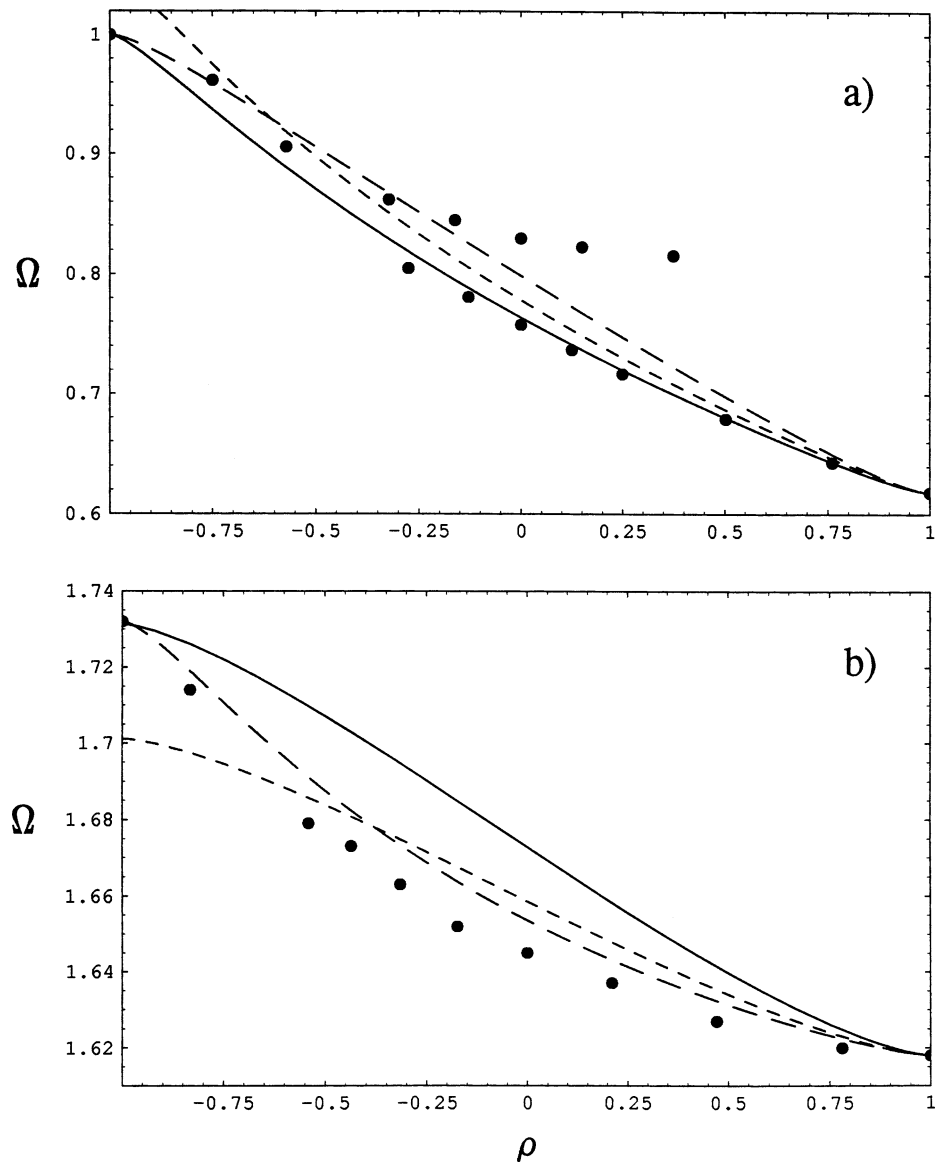

Fig. 2 Frequencies of reduced-order models of the 2-dof system with clearance nonlinearity in (a) mode 1 and (b) mode 2 computed via the linear-based reduction (*short-dashed*), PMM (*solid*), LELSM (*long-dashed*), and numerical simulation of the full model (*dots*) as a function of clearance for $\alpha^2 = 2$

full 2-dof system. It can be seen that for this value of α there are two separate branches of NNMs for mode 1.

3.2 Symmetric deadzone and saturation nonlinearities

Next, consider the n-degree-of-freedom vibrating system in Fig. 1 where the clearance is replaced with an odd symmetric deadzone or saturation nonlinearity of the form

$$f(x_1) = \begin{cases} 0; & |x_1| < x_c \\ k_c(x_1 - x_c); & x_1 > x_c \\ k_c(x_1 + x_c); & x_1 < -x_c \end{cases} \quad \text{or}$$

$$f(x_1) = \begin{cases} k_c x_1; & |x_1| < x_c \\ k_c x_c; & x_1 > x_c \\ -k_c x_c; & x_1 < -x_c \end{cases} \tag{21}$$

respectively. The stiffness of the first mass is divided into three distinct linear subregions. Since the masses' positions are measured from equilibrium, penetration of the first mass into the first and third subregion is made only when the energy of the system is sufficient such that the clearance is traversed by the first mass, i.e. $x_1 > x_c$ or $x_1 < -x_c$. Otherwise if the energy is insufficient for m_1 to reach x_c or $-x_c$, then the system remains in the second linear subregion. The scaled variables in Equation (15) are now introduced where ω_- (or ω_+) is the linear frequency of m_1 (with m_2 held still) in the second subregion and ω_+ (or ω_-) is the frequency in the first and third subregions for deadzone (or saturation, respectively).

The total period of the single-degree-of-freedom system in Equation (16) with $f(x_1)$ as in Equation (21) can be found by integrating over the closed path Γ as

$$T = \oint_\Gamma dt = 4\int_0^{x_c} \frac{1}{\dot{x}_-} dx_- + 4\int_{x_c}^{x_0} \frac{1}{\dot{x}_+} dx_+ \tag{22}$$

where the velocities are found from the phase plane $x_-^2 + \dot{x}_-^2 = \alpha^2(x_0 - x_e)^2$ and $\alpha^2(x_+ - x_e)^2 + \dot{x}_+^2 = \alpha^2(x_0 - x_e)^2$ where $x_e = (1 - 1/\alpha^2)x_c$ for deadzone. This yields the exact amplitude-dependent frequency as

$$\Omega = \omega_-\omega_+\left[\frac{2\omega_+}{\pi}\sin^{-1}\left(\frac{\rho}{\sqrt{(\rho-1)^2\alpha^2 + \rho(2-\rho)}}\right) + \omega_-\left(1 - \frac{2}{\pi}\sin^{-1}\left(\frac{\rho}{\alpha^2 - \rho(\alpha^2-1)}\right)\right)\right]^{-1} \tag{23}$$

where $\rho = x_c/x_0$ lies in the interval [0,1]. For saturation, the substitutions $\omega_+ \leftrightarrow \omega_-$ and $\alpha \to 1/\alpha$ are made in Equation (23) to obtain

$$\Omega = \omega_-\omega_+\left[\frac{2\omega_-}{\pi}\sin^{-1}\left(\frac{\rho}{\sqrt{\rho(2-\rho) + \frac{(\rho-1)^2}{\alpha^2}}}\right) + \omega_+\left(1 - \frac{2}{\pi}\sin^{-1}\left(\frac{\rho}{\frac{1}{\alpha^2} - \rho(\frac{1}{\alpha^2} - 1)}\right)\right)\right]^{-1} \tag{24}$$

Like Equation (19), Equations (23) and (24) are exact for the single-degree-of-freedom case and can be used in conjunction with the reduced-order model of Equation (12) where $\omega_- = \omega_i$ and $\omega_+ = \sqrt{\omega_i^2 + \beta_i k_c}$ to estimate the NNM frequencies. In Figs. 3 and 4, the approximate NNM frequencies in both modes of the two-degree-of-freedom systems obtained from the linear-based reduced models as well as the PMM and LELSM methods are plotted versus ρ for $\alpha^2 = 2$ along with the exact NNM frequencies found by direct numerical simulation.

Alternatively, harmonic balance may be used to obtain the frequency–amplitude dependence [19]. To the first approximation this results in

$$\Omega = \omega_-\sqrt{\alpha^2 - \frac{2}{\pi}(\alpha^2 - 1)(\sin^{-1}\rho + \rho\sqrt{1-\rho^2})} \tag{25}$$

for deadzone and

$$\Omega = \omega_-\sqrt{1 + \frac{2}{\pi}(\alpha^2 - 1)(\sin^{-1}\rho + \rho\sqrt{1-\rho^2})} \tag{26}$$

for saturation. Although these approximations are more concise and may be sufficiently accurate, it must be remembered that Equations (23)–(24) are exact for the single-degree-of-freedom system.

3.3 Bang-bang nonlinearity

Finally, consider the system in Fig. 1 where a bang-bang nonlinearity defined by

$$f(x_1) = \begin{cases} -\delta; & x_1 < 0 \\ \delta; & x_1 > 0 \end{cases} \tag{27}$$

replaces the clearance. It should be noted that crossing of the discontinuity will occur regardless of the

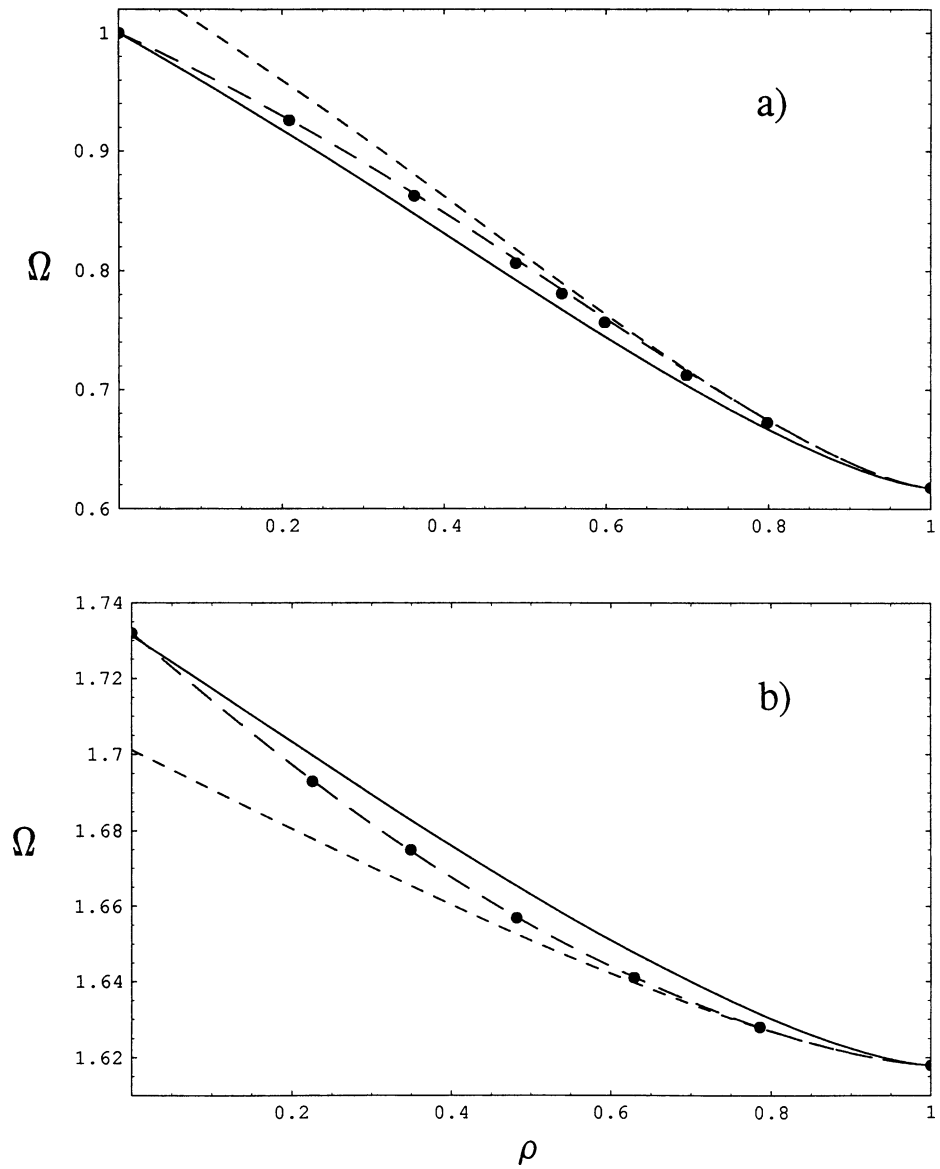

Fig. 3 Frequencies of reduced-order models of the 2-dof system with deadzone nonlinearity in (a) mode 1 and (b) mode 2 computed via the linear-based reduction (*short-dashed*), PMM (*solid*), LELSM (*long-dashed*), and numerical simulation of the full model (*dots*) for $\alpha^2 = 2$

amplitude of oscillation. By integrating over the closed path as

$$T = \oint_{\Gamma} dt = 4 \int_0^{x_0} \frac{1}{\dot{x}} dx \tag{28}$$

in terms of the closed orbits $(x - x_e)^2 + \dot{x}^2 = (x_0 + \delta/\omega^2)^2$ where $x_e = -\delta/\omega^2$, the exact frequency for the single-degree-of-freedom system in Equations (16) and (27) is found as

$$\Omega = \frac{\omega}{1 - \frac{2}{\pi}\sin^{-1}(\rho/(\rho + \omega^2))} \tag{29}$$

where ω is the frequency in both discontinuous linear subregions and $\rho = \delta/x_0$. In particular, for the single-degree-of-freedom reduced model in Equation (12)

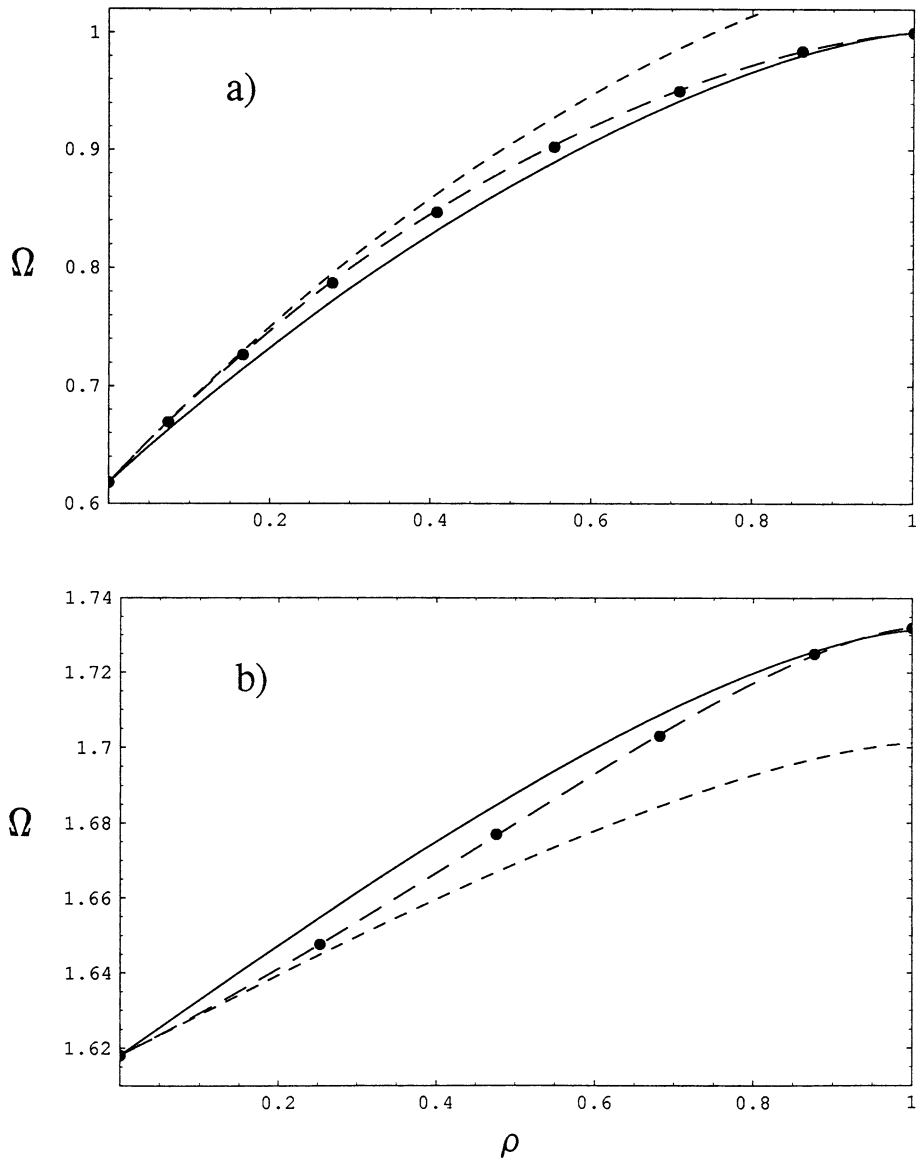

Fig. 4 Frequencies of reduced-order models of the 2-dof system with saturation nonlinearity in (a) mode 1 and (b) mode 2 computed via the linear-based reduction (*short-dashed*), PMM (*solid*), LELSM (*long-dashed*), and numerical simulation of the full model (*dots*) for $\alpha^2 = 2$

with $f(x_1)$ given in Equation (27), it is

$$\Omega_i = \frac{\omega_i}{1 - \frac{2}{\pi}\sin^{-1}\left(\frac{\beta_i \rho}{\beta_i \rho + \omega_i^2}\right)} \tag{30}$$

Equation (30) can be used to estimate the NNM frequencies. In Fig. 5, the approximate NNM frequencies in both modes of the two-degree-of-freedom system obtained from the linear-based reduced models as well as the PMM and LELSM methods are plotted versus ρ along with the exact NNM frequencies found by direct numerical simulation.

As with deadzone and saturation, the approximate relations

$$\Omega = \omega\sqrt{1 + \frac{4\rho}{\pi\omega^2}} \quad \Omega_i = \omega_i\sqrt{1 + \frac{4\beta_i\rho}{\pi\omega_i^2}} \tag{31}$$

obtained via harmonic balance may be used instead of Equations (29) and (30).

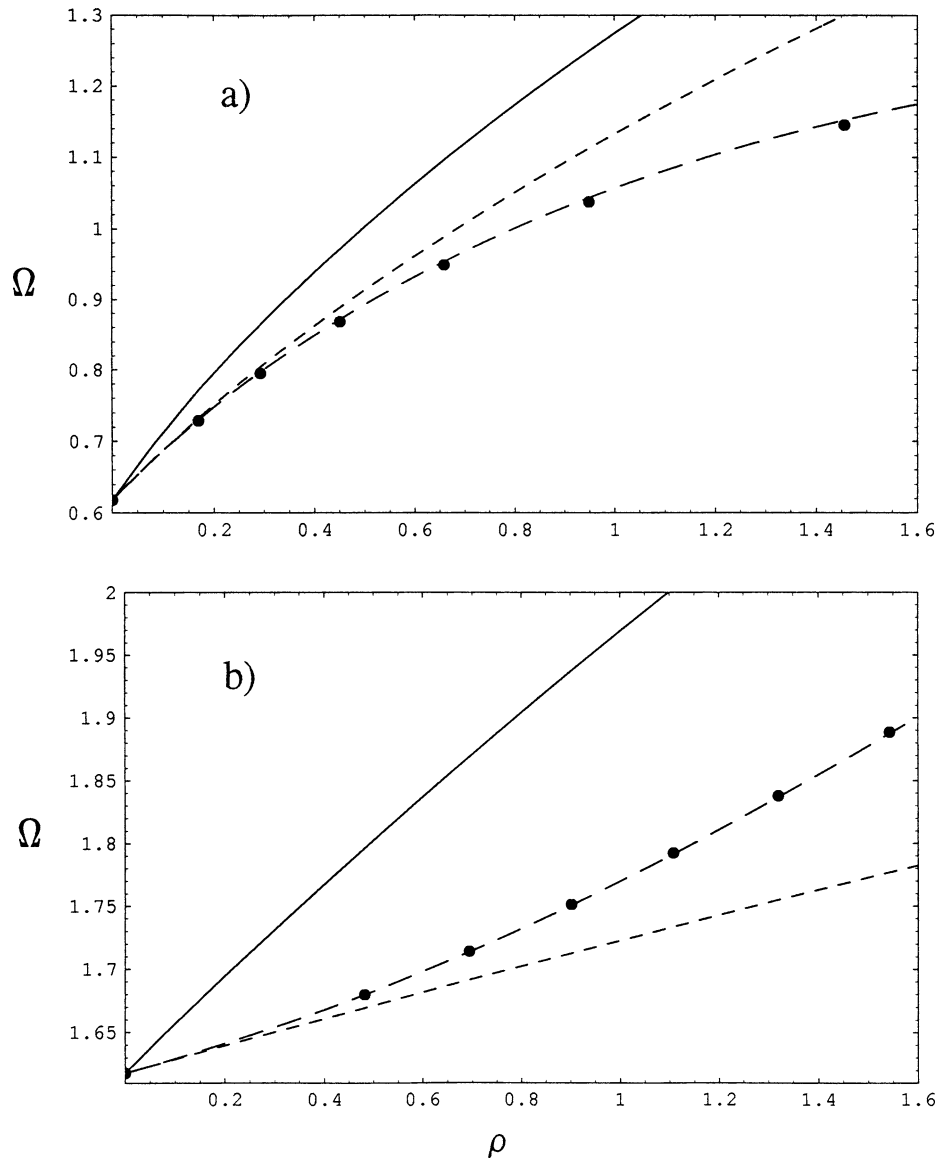

Fig. 5 Frequencies of reduced-order models of the 2-dof system with bang-bang nonlinearity in (a) mode 1 and (b) mode 2 computed via the linear-based reduction (*short-dashed*), PMM (*solid*), LELSM (*long-dashed*), and numerical simulation of the full model (*dots*)

4 Improved reduced-order model via PMM

Figures 2–5 show that, for significant ranges of the parameter ρ in one or both modes, the PMM or LELSM methods more accurately approximate the true NNM frequency than does the exact frequency of the single-degree-of-freedom linear-based reduced model. Therefore, it is possible that an alternate value of β_i in Equation (12) can be derived from the PMM or LELSM methods which could result in an improved reduced model. First, reconsider the multiple degree-of-freedom system in Fig. 1 with the bilinear clearance nonlinearity. The PMM method approximates the BNM frequencies in the ith mode from two

separate sets of eigenfrequencies by direct analogy to Equations (19) or (20) as [9]

$$\Omega_i = 2\omega_{-i}\omega_{+i}\left[\omega_{+i}\left(1+\frac{2}{\pi}\sin^{-1}\rho\right)+\omega_{-i}\left(1-\frac{2}{\pi}\sin^{-1}\left(\frac{\rho}{\gamma_i\sqrt{1-\rho^2(1-\frac{1}{\gamma_i^2})}}\right)\right)\right]^{-1}$$
$$= 2\omega_{-i}\left[1+\frac{2}{\pi}\sin^{-1}\rho+\frac{1}{\gamma_i}\left(1-\frac{2}{\pi}\times\sin^{-1}\left(\frac{\rho}{\gamma_i\sqrt{1-\rho^2(1-\frac{1}{\gamma_i^2})}}\right)\right)\right]^{-1} \quad (32)$$

(for a nonvanishing clearance) and

$$\Omega_i = \frac{2\omega_{-i}\omega_{+i}}{\omega_{+i}+\omega_{-i}} = \frac{2\omega_{-i}}{1+1/\gamma_i} \quad (33)$$

(for a vanishing clearance), respectively, where $\gamma_i = \omega_{+i}/\omega_{-i}$ is the ratio of frequencies in the ith mode in the two linear subregions. Equation (33) was used by Chati et al. [8] for a multi-degree-of-freedom bilinear system with vanishing clearance. In this special case, the bilinear frequencies are independent of the amplitude. PMM approximates the BNM manifold as the piecewise union of the separate eigenvectors in the two linear subregions joined at the boundary. (However, for a nonvanishing clearance the eigenvectors do not match continuously at the boundary.) Equation (32) was used to estimate the NNM frequencies in Fig. 2 via PMM. For deadzone, this relation is found by direct analogy to Equation (23) as

$$\Omega_i = \omega_{-i}\left[\frac{2}{\pi}\sin^{-1}\left(\frac{\rho}{\sqrt{\rho(2-\rho)+(\rho-1)^2\gamma_i^2}}\right)+\frac{1}{\gamma_i}\left(1-\frac{2}{\pi}\sin^{-1}\left(\frac{\rho}{\gamma_i^2-\rho(\gamma_i^2-1)}\right)\right)\right]^{-1} \quad (34)$$

while for saturation it is found by analogy to Equation (24) as

$$\Omega_i = \omega_{-i}\left[\frac{2}{\gamma_i\pi}\sin^{-1}\left(\frac{\rho}{\sqrt{\rho(2-\rho)+\frac{(\rho-1)^2}{\gamma_i^2}}}\right)+1-\frac{2}{\pi}\sin^{-1}\left(\frac{\rho}{\frac{1}{\gamma_i^2}-\rho\left(\frac{1}{\gamma_i^2}-1\right)}\right)\right]^{-1} \quad (35)$$

Equations (34) and (35) were used to estimate the NNM frequencies in Figs. 3 and 4 via PMM. Alternatively, the harmonic balance relations in Equations (25) and (26) may be used in PMM instead.

Let us try to find an improved value of β_i in the reduced model of Equation (12) via PMM for each of these nonlinearities. For clearance, deadzone, and saturation, the ith linear frequency in the second subregion is $\omega_{+i} = \sqrt{\omega_{-i}^2+\beta_i k_c}$. Since both sets of linear frequencies can be easily determined, an improved value of β_i which is independent of the amplitude can be found easily as

$$\beta_i = \frac{1}{k_c}\left(\omega_{+i}^2-\omega_{-i}^2\right) \quad (36)$$

for these nonlinearities. It is seen in Fig. 2 that the PMM-based reduced model for clearance is a substantial improvement over the linear-based one for a wide range of ρ in the first mode (especially for the lower branch) only. In Fig. 3, it is seen that PMM offers improvement for deadzone for small ρ values only, while from Fig. 4 it is seen that this is true for saturation for high values of ρ.

For bang-bang, the PMM relation for the ith NNM frequency is found by analogy with Equation (29) as

$$\Omega_i = \frac{\omega_i}{1-\frac{2}{\pi}\sin^{-1}\left(\frac{\rho}{\rho+\omega_i^2}\right)} \quad (37)$$

or, alternatively, with Equation (31). Equation (37) was used to estimate the NNM frequencies in Fig. 5 via PMM. To use PMM in the reduced model of Equation (12), therefore, it is seen that $\beta_i = 1$ in Equation (30) or (31). It is seen in Fig. 5 that the corresponding reduced models will be improved over the linear-based reduced models only in the first mode.

5 Improved reduced-order models via LELSM

Another route for estimating the NNM frequencies is to construct an equivalent linear vibrating system whose eigenfrequencies approximate the NNM frequencies of the full model. For this purpose, it was recognized in [9] that, for a single nonsmooth nonlinearity, one element in the linear stiffness matrix can be

altered according to the effect of the nonlinearity on the frequency of the single-degree-of-freedom system with the corresponding mass while holding the others at equilibrium. Therefore, the local equivalent linear stiffness method (LELSM) is based on constructing an equivalent linear stiffness matrix $\boldsymbol{K}_{\text{eq}}$ in which the elements of $\boldsymbol{K}$ that change with linear subregions are replaced by a constant $k_{\text{eq}} = \Omega^2$. Here, Ω is the exact frequency of the single-degree-of-freedom system given by Equations (19), (23), (24) and (29) while k_{eq} is the equivalent linear stiffness which causes that system to vibrate with the same frequency. The solution of the eigenvalue problem $|\boldsymbol{K}_{\text{eq}} - \Omega_i^2 \boldsymbol{I}| = 0$ then yields the approximate NNM frequencies Ω_i in each mode. Note that, as in PMM, the Ω_i are amplitude-dependent through the variable ρ in k_{eq} and the results for the limiting linear cases ($\rho = \pm 1$ for clearance; $\rho = 0, 1$ for deadzone and saturation; $\rho = 0$ for bang-bang) are exact. The LELSM frequency estimates in Figs. 2–5 were produced in this way. As can be seen in these figures, this method can be used to obtain improved reduced-order models whose frequencies are more accurate than those obtained from the linear-based reduced models for clearance (mode 2 only) and deadzone, saturation, and bang-bang (both modes).

In order to find the value of β_i using the LELSM estimate of the NNM frequency Ω_i for clearance, deadzone, and saturation, we substitute the relation $\gamma_i = \sqrt{\omega_{-i}^2 + \beta_i k_c}/\omega_{-i}$ in Equations (32)–(35) and numerically solve the transcendental equation for β_i once Ω_i is estimated via LELSM. (Note that in the case of vanishing clearance, Equation (33) can be solved analytically for β_i.) For a bang-bang nonlinearity, Equation (30) can be solved analytically for β_i. An alternative for the odd symmetric nonlinearities is to use the harmonic balance relations in Equations (25) and (26) with $\alpha = \gamma_i = \sqrt{\omega_{-i}^2 + \beta_i k_c}/\omega_{-i}$ or Equation (31) to obtain the improved nonlinearity parameter β_i analytically. The reduced models obtained in this paper (which are dependent on the amplitudes) utilized the exact relations in Equations (34), (35) and (37).

It is seen in Figs. 3–5 that LELSM is extremely accurate in predicting the NNM frequencies for odd symmetric nonsmooth nonlinearities (deadzone, saturation, and bang-bang) in particular.

Additionally, the eigenvectors of $\boldsymbol{K}_{\text{eq}}$ are good approximations for the NNM invariant manifolds in the least-squares sense similar to principal orthogonal modes (POMs). This approximation is more successful for the odd symmetric nonlinearities whose invariant manifolds pass through the origin than for the bilinear clearance. In Figs. 6–8, the slopes of the LELSM eigenvectors for the systems with odd symmetric nonlinearities are shown in both modes versus the parameter ρ along with the slopes of the best-fit lines determined by least-squares regression of the numerically integrated NNM manifolds. Although it was shown in [20, 21] that POMs are the optimal least-squares linear approximations to NNM invariant manifolds for systems with smooth nonlinearities, it must be noted that, because $\boldsymbol{K}_{\text{eq}}$ is amplitude-dependent, it corresponds to a particular mode. For a given total energy, each mode in general has a separate $\boldsymbol{K}_{\text{eq}}$ matrix from which the corresponding eigenvector is the best linear approximation for that mode, and these eigenvectors are not orthogonal. (Some higher modes which do not penetrate a boundary of stiffness discontinuity remain linear.) Hence, these eigenvectors accurately capture an important trait of NNMs of nonsmooth systems: *in general, they are not orthogonal at their intersection* [6]. Hence, although the LELSM eigenvectors are not strictly the POMs of the system, they are even more accurate in approximating the individual NNM manifolds with a linear mode shape. This in turn enables improved master – slave relationships to be obtained which are more accurate than the linear-based ones used in Section 2. Unlike PMM, LELSM can accommodate multiple nonsmooth nonlinearities with several surfaces of discontinuity, similarly to the use of describing functions where individual nonlinearities in the system are translated into equivalent linear gains.

6 Examples

6.1 Bilinear clearance nonlinearity

The system in Equation (14) with $n = 2$ is again considered where $m_1 = m_2 = k_1 = k_2 = 1$. To find the exact frequencies by numerical integration, the BNMs can be located by simulating the motion for variety of initial conditions along the equipotential boundary

$$E = \begin{cases} \left(x_2^2 + (x_1 - x_2)^2\right)/2; & x_1 < x_c \\ \left(x_2^2 + (x_1 - x_2)^2 + \kappa_c (x_1 - x_c)^2\right)/2; & x_1 > x_c \end{cases} \tag{38}$$

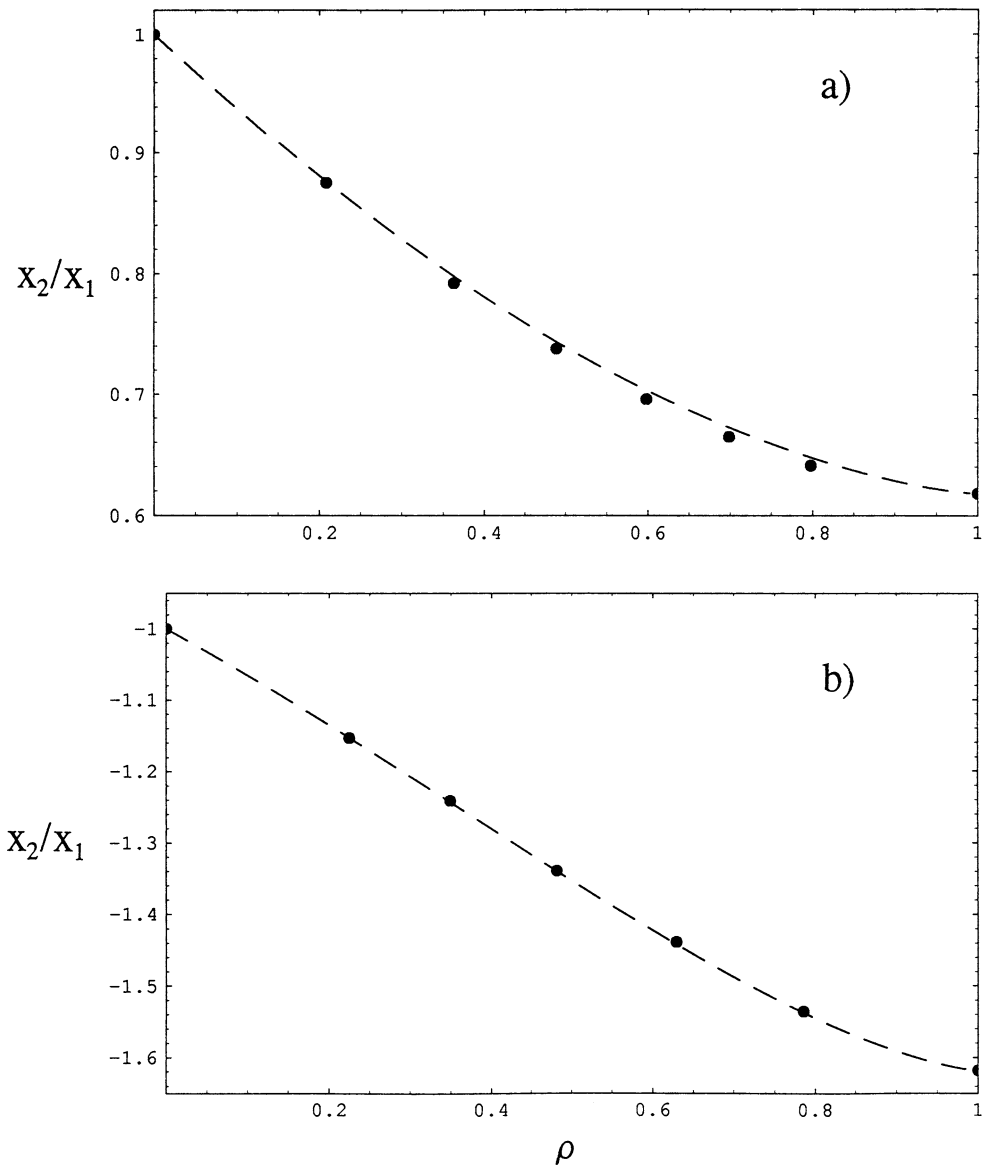

Fig. 6 Slopes of the LELSM eigenvectors (*long-dashed*) of the 2-dof system with deadzone nonlinearity in (a) mode 1 and (b) mode 2 for $\alpha^2 = 2$. For comparison, the slopes of the best-fit lines determined via least-squares regression of the numerically simulated NNM manifolds are also shown (*dots*)

corresponding to some chosen energy level. Through trial and error, the correct initial conditions which yield periodic motion can be located by examining the motion in the configuration space. This is shown in Fig. 9 where the free spring has the same stiffness as the coupling springs ($k_c = 1$ or $\alpha^2 = 2$) and the total energy is $E = 1$ for several different values for the clearance x_c. The first (a) and last (i) plots correspond to the two linear subregions $\rho = 1$ and -1, respectively, while the BNM frequencies in (e) (where $\rho = 0$) are independent of the amplitude. As was also shown in Fig. 3, it s seen here that the nonlinearity is strong enough such that three period 1 BNMs are present for some clearance values (e,f,g). These characteristics were first reported for this system in [9].

The linear mode shapes in the first subregion are $\phi_1 = (1.0\ 0.618)^{\mathrm{T}}$ and $\phi_2 = (1.0\ -1.618)^{\mathrm{T}}$ and the modal frequencies are $\omega_1 = 0.618$ and $\omega_2 = 1.618$. The linear-based order reduction transformation of Equation (11) results in the reduced model

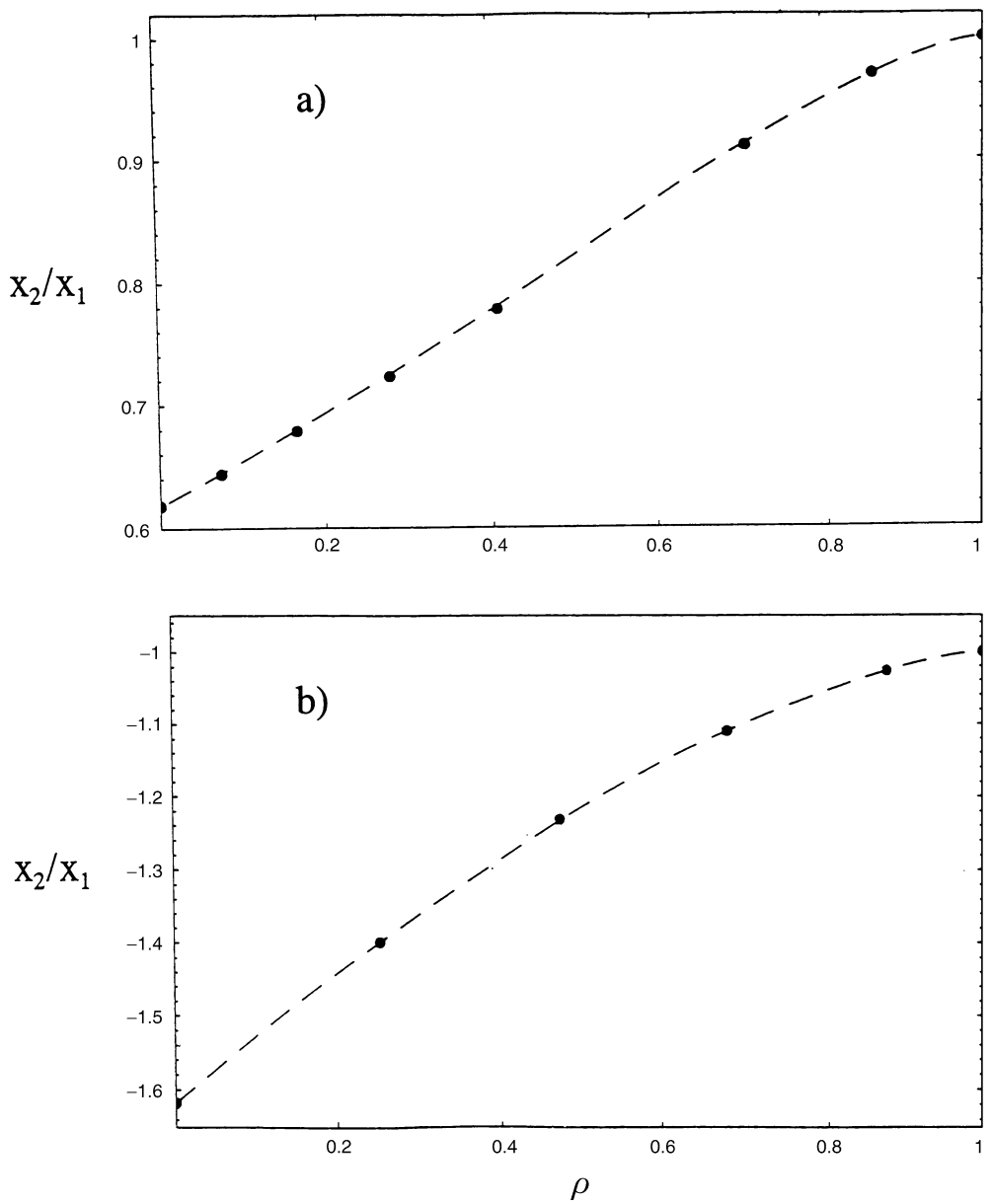

Fig. 7 Slopes of the LELSM eigenvectors (*long-dashed*) of the 2-dof system with saturation nonlinearity in (a) mode 1 and (b) mode 2 for $\alpha^2 = 2$. For comparison, the slopes of the best-fit lines determined via least-squares regression of the numerically simulated NNM manifolds are also shown (*dots*)

of Equation (12) where $\beta_1 = 0.724$ in the first mode and $\beta_2 = 0.276$ in the second. We compare the various reduced models with the exact BNM frequencies as a function of the dimensionless parameter ρ. For the case of $x_c = 0.5$ (Fig. 9d) the exact first modal frequency is found by numerical simulation to be 0.717 rad/s.

Using Equation (19), the approximate nonlinear frequency obtained from the linear-based reduced model is 0.730 rad/s. Hence, time series plots of both coordinates for the full and reduced-order models become 180° out of phase in 242 s as is shown explicitly in Fig. 10. However, PMM can be used to obtain the improved reduced model

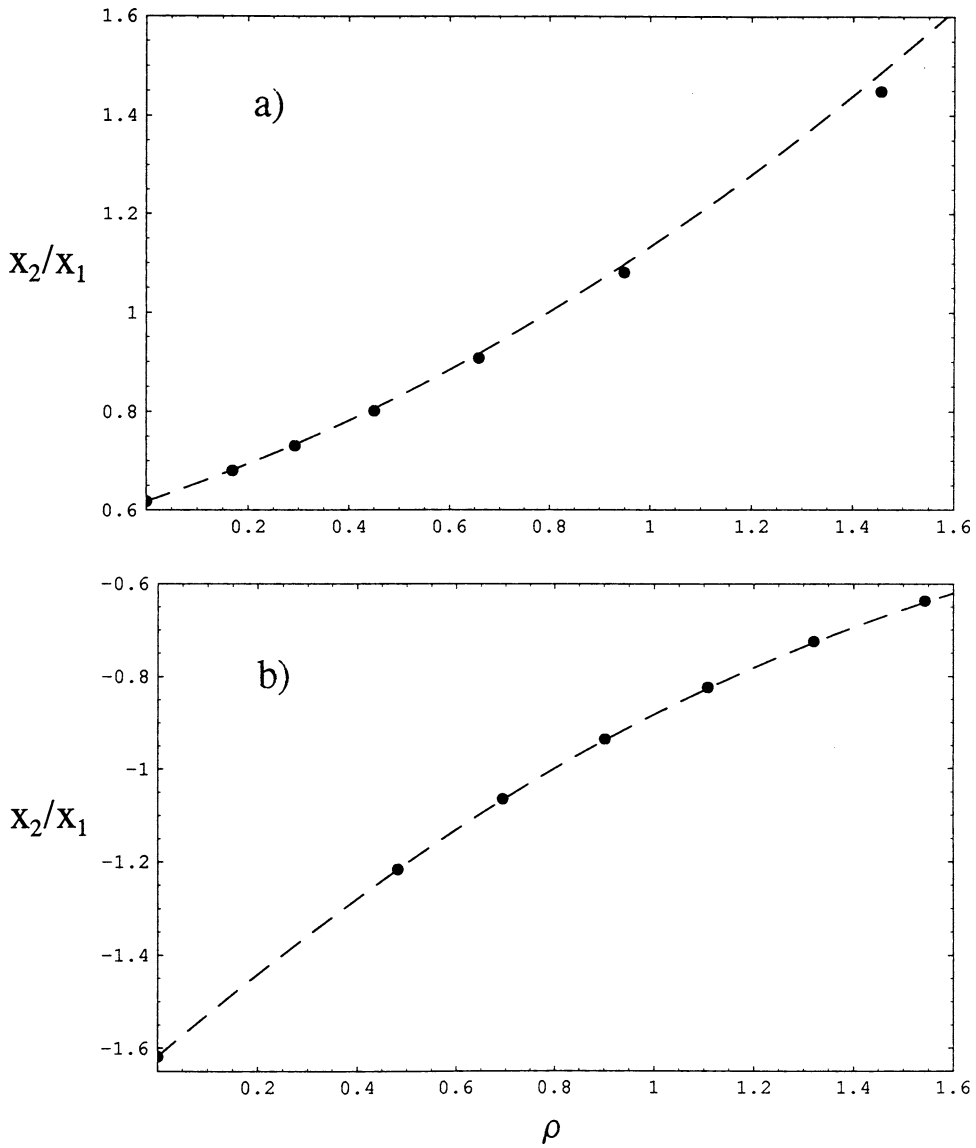

Fig. 8 Slopes of the LELSM eigenvectors (*long-dashed*) of the 2-dof system with bang-bang nonlinearity in (a) mode 1 and (b) mode 2 for $\alpha^2 = 2$. For comparison, the slopes of the best-fit lines determined via least-squares regression of the numerically simulated NNM manifolds are also shown (*dots*)

$$\ddot{x}_1 + 0.618^2 x_1 + 0.618 f(x_1) = 0 \tag{39}$$

(where $\beta_1 = 0.618$ was found via Equation (36) and is independent of the amplitude) which has a frequency of 0.720 rad/s. Figure 10 shows that the corresponding motion remains closer in phase with that of the full model since it now takes 1047 s to become 180° out of phase. Thus, this amplitude-independent reduced-order model, which is easily obtained without the simulation of the full model, represents a significant improvement over the linear-based version.

Figure 2 shows that LELSM is much better at approximating the BNM frequencies in the second mode than PMM. The equivalent linear stiffness matrix in this method is given by

$$K_{\text{eq}} = \begin{bmatrix} k_{\text{eq}} & -1 \\ -1 & 2 \end{bmatrix} \tag{40}$$

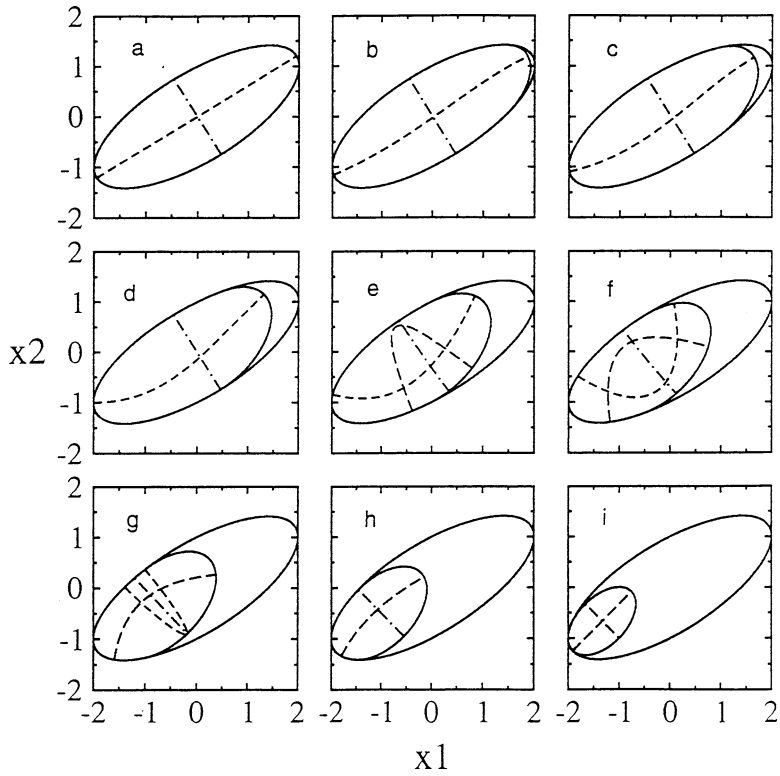

Fig. 9 Numerical simulations in configuration space of BNMs for the two-degree-of-freedom system with clearance nonlinearity with $\alpha^2 = 2$ and $x_c =$ (a) 2.0 (*linear*) (b) 1.5 (c) 1.0 (d) 0.5 (e) 0.0 (f) -0.5 (g) -1.0 (h) -1.5 (i) -2.0 (*linear*). The solid closed curves are the equipotential boundaries with and without the nonlinear spring

where k_{eq} is found from

$$k_{\text{eq}} = \Omega^2 = 4\omega_-^2\left[1 + \frac{2}{\pi}\sin^{-1}\rho + \frac{1}{\alpha}\left(1 - \frac{2}{\pi}\times \sin^{-1}\left(\frac{\rho}{\alpha\sqrt{1-\rho^2\left(1-\frac{1}{\alpha^2}\right)}}\right)\right)\right]^{-2} \quad (41)$$

with $\alpha^2 = 2$ and $\omega_- = 1$. Unlike Equation (39) a LELSM-based reduced model is amplitude-dependent as is shown in the next section. Hence, in general, if it is desired that the reduced model should portray the dynamics of higher modes in a system with a bilinear clearance nonlinearity, LELSM can yield improved reduced-order models. It should be noted that the LELSM-based results in Fig. 2 are more accurate than those in [9].

6.2 Deadzone nonlinearity

As an example of a system with deadzone nonlinearity, the equations of motion for the two-degree-of-freedom version of Equations (14) and (21) are considered where $m_1 = m_2 = k_1 = k_2 = 1$. The configuration space plots obtained by numerical simulation for $\alpha^2 = 2$ are shown in Fig. 11 for four values of x_c along with the equipotential boundary

$$E = \begin{cases} \left(x_2^2 + (x_1 - x_2)^2\right)/2; & |x_1| < x_c \\ \left(x_2^2 + (x_1 - x_2)^2 + \kappa_c(x_1 - x_c)^2\right)/2; & x_1 > x_c \\ \left(x_2^2 + (x_1 - x_2)^2 + \kappa_c(x_1 + x_c)^2\right)/2; & x_1 < -x_c \end{cases} \quad (42)$$

for $E = 1$. The first (a) and last (d) plots correspond to the two linear subregions $\rho = 0$ and 1, respectively. Unlike the clearance case, the number of NNMs is equal to the number of degrees of freedom for all values of ρ.

The linear-based order reduction transformation in Equation (11) results in the reduced model of Equation (12) with the same values for β_1 and β_2 as in the clearance example. For the case of $x_c = 0.5$ (Fig. 11b), the exact first modal frequency found from numerical simulation is 0.862 rad/s. Using Equation (23), the frequency obtained from the linear-based reduced model is 0.880 rad/s. An improved reduced model, however, can be obtained via LELSM. The

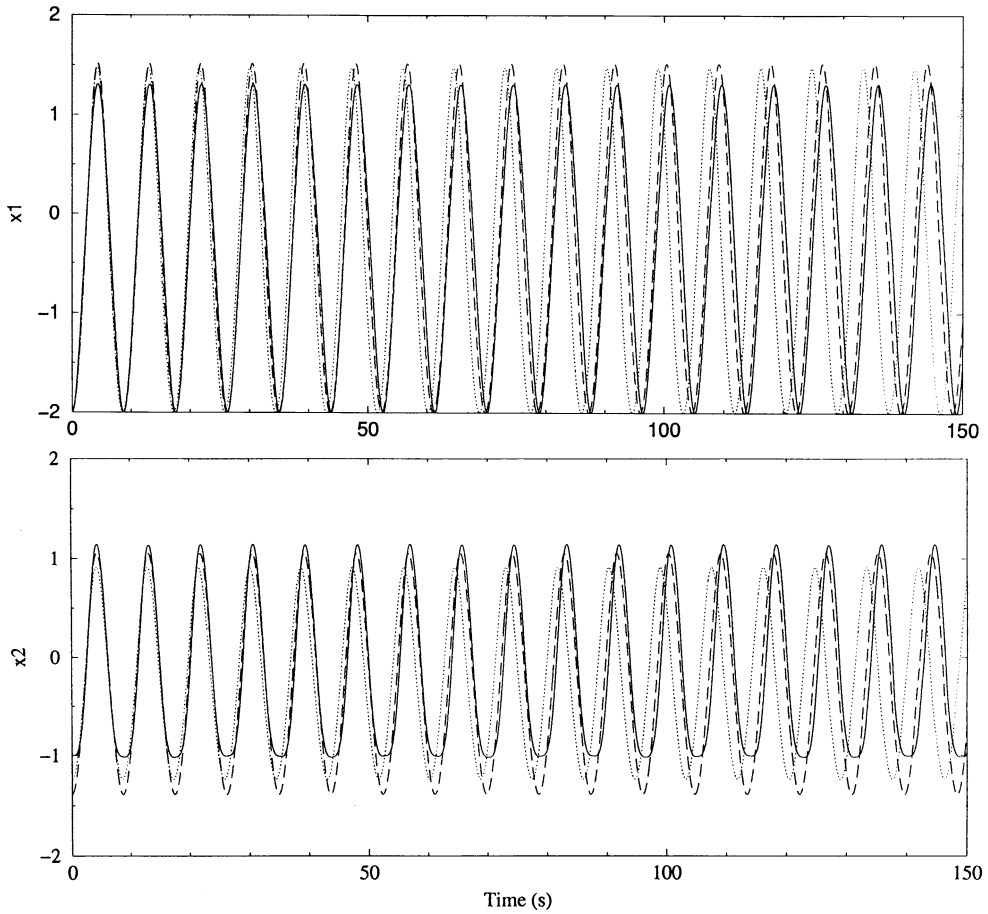

Fig. 10 Time series of reduced-order models of the 2-dof system with clearance nonlinearity in the first mode computed via the linear-based reduction (*dotted*), PMM (*dashed*), and numerical simulation of the full model (*solid*) for $\alpha^2 = 2$ and $x_c = 0.5$

equivalent linear stiffness matrix in this method is given by Equation (40) where k_{eq} is found from

$$k_{eq} = \omega_-^2 \left[\frac{2}{\pi} \sin^{-1} \frac{\rho}{\sqrt{(\rho-1)^2\alpha^2 + \rho(2-\rho)}} + \frac{1}{\alpha}\left(1 - \frac{2}{\pi}\sin^{-1}\left(\frac{\rho}{\alpha^2 - \rho(\alpha^2-1)}\right)\right)\right]^{-2} = 1.545 \tag{43}$$

with $\alpha_2 = 2, \omega_- = 1$, and $\rho = 0.363$ (using the amplitude of 1.377 for mass 1 found from simulation of the first NNM). The relation $|\boldsymbol{K}_{\text{eq}} - \Omega_i^2 \boldsymbol{I}| = 0$ then results in a frequency of $\Omega_1 = 0.864$ which is much closer to the exact one. As described in Section 5, we may obtain $\beta_1 = 0.671$ for the corresponding improved reduced-order model given by

$$\ddot{x}_1 + 0.618^2 x_1 + 0.671 f(x_1) = 0 \tag{44}$$

In addition, we may obtain the improved master–slave relation $x_2 = 0.798 x_1$ from the eigenvector $(1.0, 0.798)$ of $\boldsymbol{K}_{\text{eq}}$. Thus, the solution for x_2 is obtained from that of x_1 in the reduced model. Comparisons of exact, linear-based, and improved results are in the time series plots in Fig. 12. As seen here, the improved reduced model obtained via LELSM results in a significant improvement in the NNM frequency and amplitude for x_2 over the linear-based reduced model.

Although the amplitude-dependent reduced model in Equation (44) was obtained using the amplitude found by simulation of the full model (for the given total energy) in advance, this amplitude may be

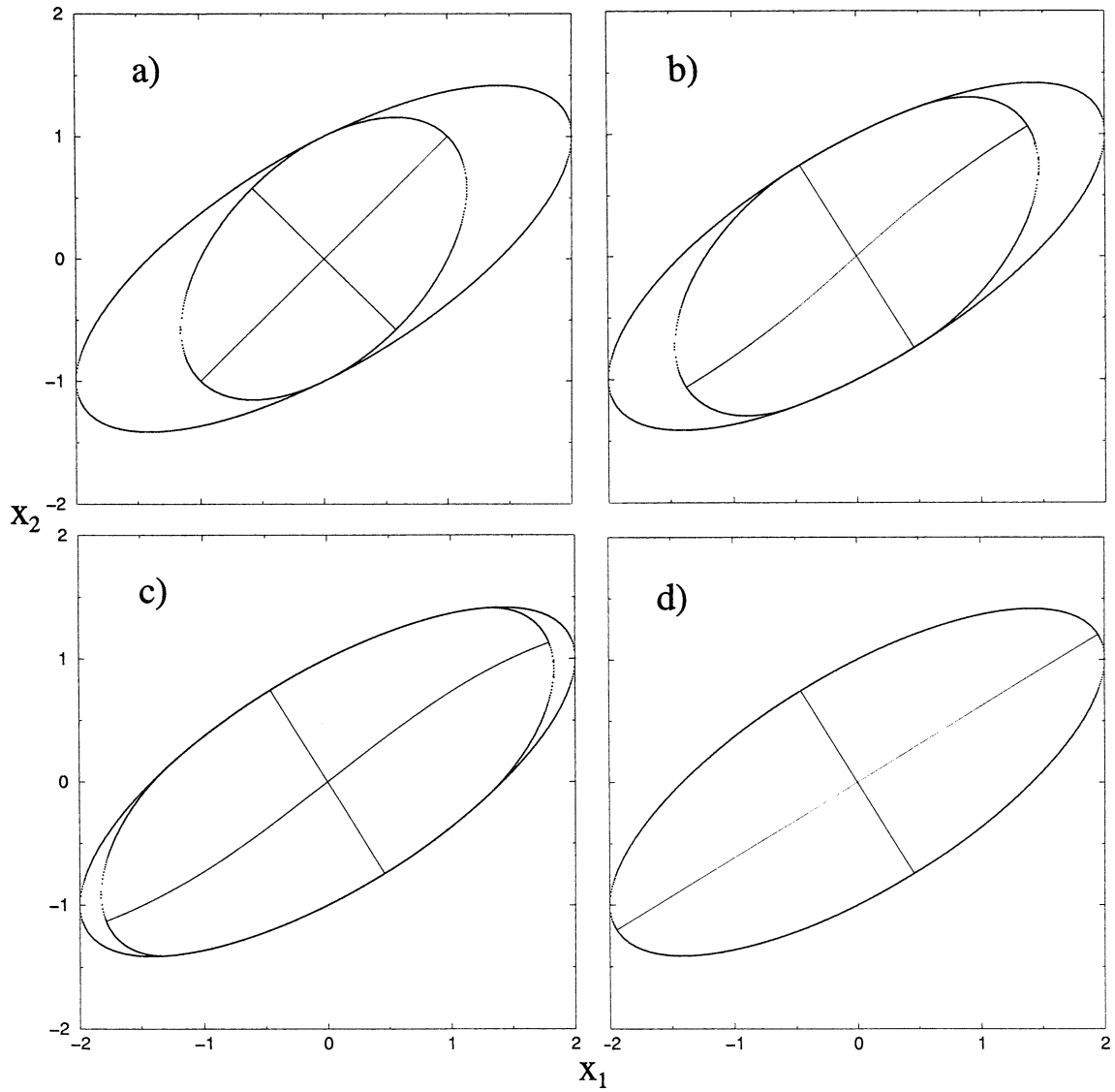

Fig. 11 Numerical simulations in configuration space of NNMs for the two-degree-of-freedom system with deadzone nonlinearity with $\alpha^2 = 2$ and $x_c =$ (a) 0.0 (*linear*) (b) 0.5 (c) 1.25 (d) 2.0 (*linear*). The solid closed curves are the equipotential boundaries with and without the nonlinear spring

approximated by the following method so that the simulation is not required. By solving for the intersections of the eigenvectors of the $\boldsymbol{K}_{\text{eq}}$ matrix with the equipotential boundaries corresponding to a given energy level, the approximate amplitude of x_1 in mode 1 is obtained. We can start by assuming the NNM occurs along the first eigenvector of the system in the first linear subregion, i.e. $\hat{x} = (1.0,\ 0.618)$. This intersects the equipotential boundary $E = \frac{1}{2}\hat{x}^T K \hat{x} + \frac{1}{2}(\hat{x}_1 - x_c)^2 = 1$ in the second linear subregion at $x_1 = 1.446$ from which $\rho = 0.346$. This can in turn be used in Equations (43) and (40) to obtain a $\boldsymbol{K}_{\text{eq}}$ whose first eigenvector intersects the equipotential boundary at $x_1 = 1.357$ from which $\rho = 0.368$. One more iteration converges at $x_1 = 1.362$ and $\rho = 0.367$, which are close approximations to the exact values of $x_1 = 1.377$ and $\rho = 0.363$ used above.

6.3 Saturation nonlinearity

For the two-degree-of-freedom system with saturation nonlinearity, the configuration space plots found by numerical simulation are shown in Fig. 13 where the

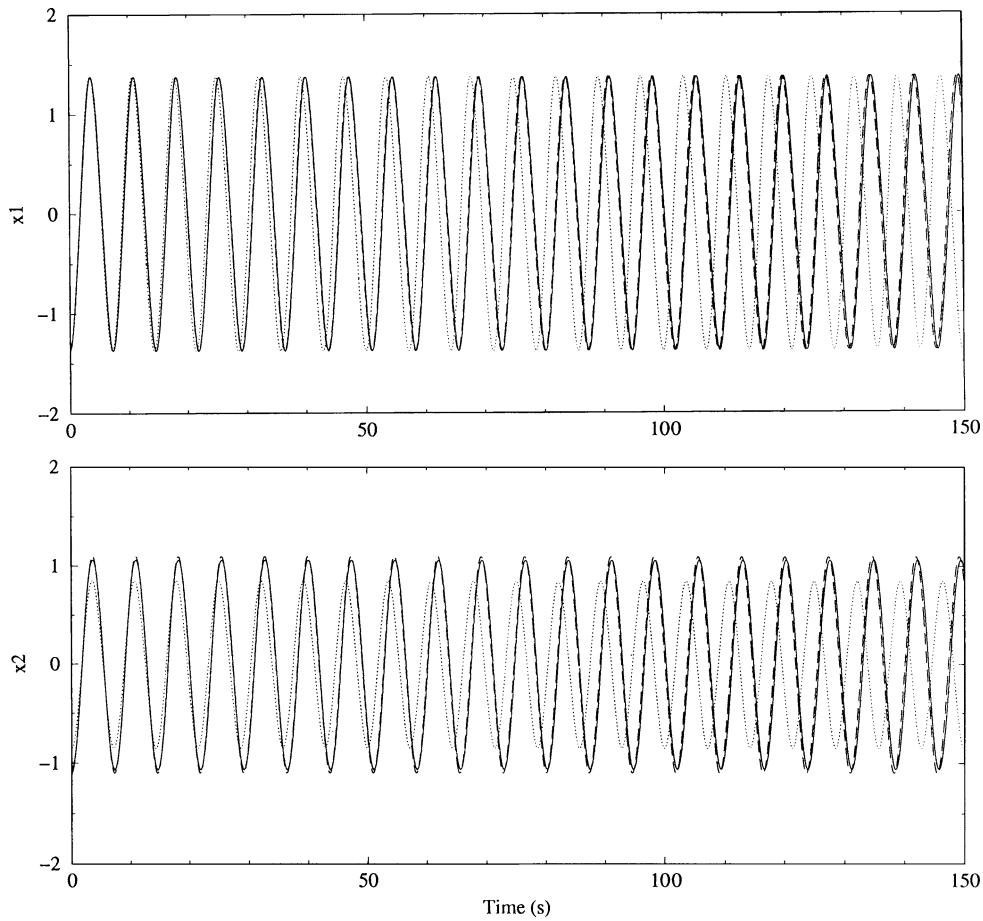

Fig. 12 Time series of reduced-order models of the 2-dof system with deadzone nonlinearity in the first mode computed via the linear-based reduction (*dotted*), LELSM (*dashed*), and numerical simulation of the full model (*solid*) for $\alpha^2 = 2$ and $x_c = 0.5$

equipotential boundary is given by

$$E = \begin{cases} \left(x_2^2 + (x_1 - x_2)^2 + \kappa_c x_1^2\right)/2; & |x_1| < x_c \\ \left(x_2^2 + (x_1 - x_2)^2 + \kappa_c x_c^2\right)/2 & |x_1| > x_c \end{cases} \tag{45}$$

for $E = 1$. The first (a) and last (d) plots correspond to the two linear subregions $\rho = 0$ and 1, respectively.

For the case of $x_c = 0.75$ (Fig. 13c), the exact first modal frequency is found to be 0.950 rad/s. from numerical simulation. The frequency obtained from the linear-based reduced model is 0.986 rad/s. An amplitude-dependent improved reduced model

$$\ddot{x}_1 + 0.618^2 x_1 + 0.640 f(x_1) = 0 \tag{46}$$

obtained via LELSM results in a frequency of $\Omega_1 = 0.951$. The improved master–slave relation is $x_2 = 0.913 x_1$. Comparisons of exact, linear-based, and improved results are in the time series plots in Fig. 14.

6.4 Bang-bang nonlinearity

For the two-degree-of-freedom system with bang-bang nonlinearity, the configuration space plots found by numerical simulation are shown in Fig. 15 where the equipotential boundary is

$$E = \begin{cases} \left(x_2^2 + (x_1 - x_2)^2\right)/2 - \delta x_1; & x_1 < 0 \\ \left(x_2^2 + (x_1 - x_2)^2\right)/2 + \delta x_1; & x_1 > 0 \end{cases} \tag{47}$$

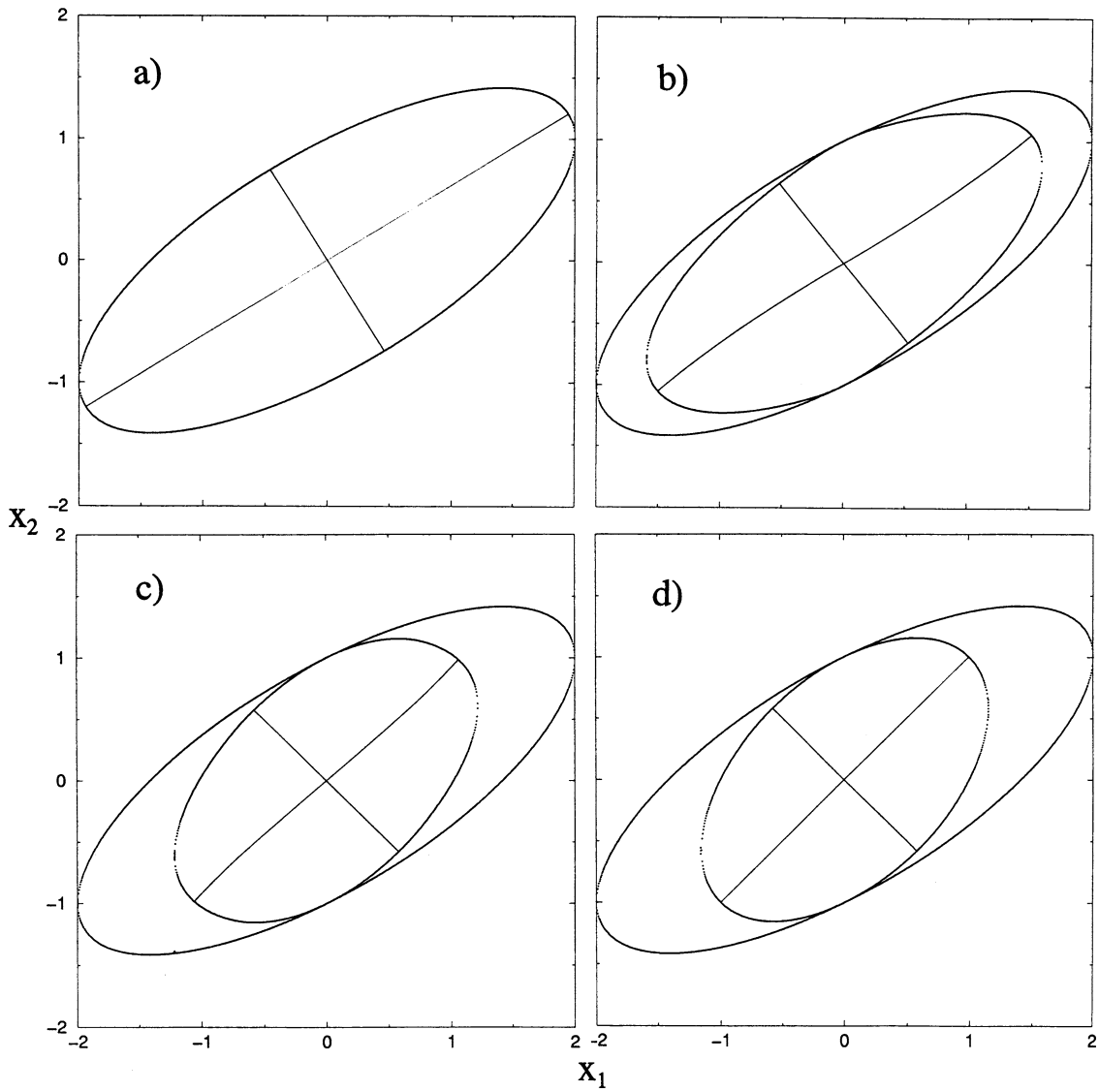

Fig. 13 Numerical simulations in configuration space of NNMs for the two-degree-of-freedom system with saturation nonlinearity with $\alpha^2 = 2$ and $x_c =$ (a) 0.0 (*linear*) (b) 0.25 (c) 0.75 (d) 1.25 (*linear*). The solid closed curves are the equipotential boundaries with and without the nonlinear spring

for $E = 1$. The first (a) plot corresponds to the linear subregion $\rho = 0$. For the case of $\delta = 0.5$ (Fig. 15c), the exact first modal frequency found from numerical simulation is 0.868 rad/s. Using Equation (28), the frequency obtained from the linear-based reduced model is 0.889 rad/s. An amplitude-dependent improved reduced model

$$\ddot{x}_1 + 0.618^2 x_1 + 0.670 f(x_1) = 0 \tag{48}$$

obtained via LELSM results in a frequency of $\Omega_1 = 0.872$. The improved master-slave relation is $x_2 = 0.806 x_1$. Comparisons of exact, linear-based, and improved results are in the time series plots in Fig. 16. As with the deadzone and saturation nonlinearities the improved reduced model obtained via LELSM for bang-bang is extremely accurate. For all values of ρ in both modes for these odd-symmetric nonlinearities, LELSM gives much better approximations than the linear-based model.

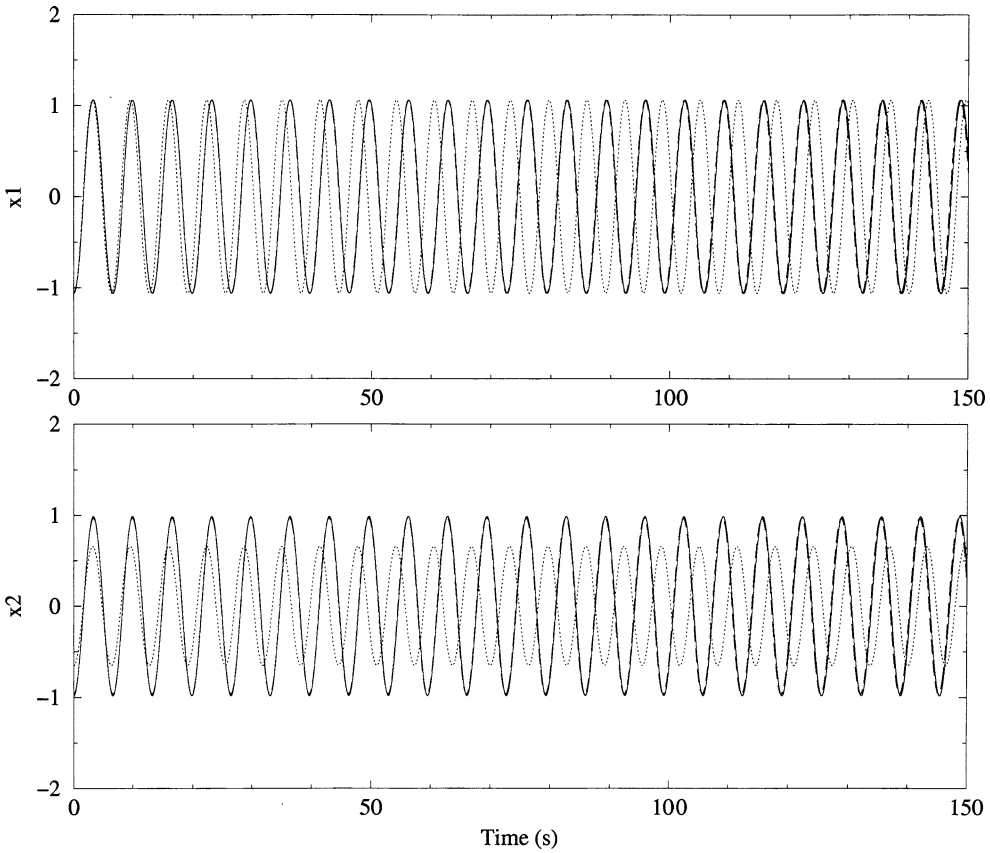

Fig. 14 Time series of reduced-order models of the 2-dof system with saturation nonlinearity in the first mode computed via the linear-based reduction (*dotted*), LELSM (*dashed*), and numerical simulation of the full model (*solid*) for $\alpha^2 = 2$ and $x_c = 0.75$

7 Reduction to multi-mode reduced models with multiple nonsmooth nonlinearities

While the examples discussed thus far involve obtaining a single-degree-of-freedom reduced model corresponding to a single NNM, it is also possible to reduce a higher-order system down to two or more degrees of freedom with dynamics approximating that of multiple NNMs. For this purpose, the LELSM method is used to obtain an equivalent linear stiffness matrix which approximates the NNM frequencies and invariant manifolds of the full model. This characteristic allows us to obtain a multi-mode reduced model which accurately approximates the true NNM manifolds projected onto the space of retained coordinates. In addition, it is also possible to accommodate multiple nonsmooth nonlinearities with several surfaces of discontinuity, as the following example shows.

Consider the four-degree-of-freedom damped system with two deadzone nonlinearities

$$\begin{bmatrix} \ddot{x}_1 \\ \ddot{x}_2 \\ \ddot{x}_3 \\ \ddot{x}_4 \end{bmatrix} + \begin{bmatrix} 0.1 & -0.1 & 0 & 0 \\ -0.1 & 0.2 & -0.1 & 0 \\ 0 & -0.1 & 0.2 & -0.1 \\ 0 & 0 & -0.1 & 0.2 \end{bmatrix} \begin{bmatrix} \dot{x}_1 \\ \dot{x}_2 \\ \dot{x}_3 \\ \dot{x}_4 \end{bmatrix} + \begin{bmatrix} 1 & -1 & 0 & 0 \\ -1 & 2 & -1 & 0 \\ 0 & -1 & 2 & -1 \\ 0 & 0 & -1 & 2 \end{bmatrix} \begin{bmatrix} x_1 \\ x_2 \\ x_3 \\ x_4 \end{bmatrix} + \begin{bmatrix} f_1(x_1) \\ f_2(x_2) \\ 0 \\ 0 \end{bmatrix} = 0 \tag{49}$$

where $f_1(x_1)$ is given by Equation (21) with $k_c = 1$ and $x_{c1} = 1.25$ and $f_2(x_2)$ is similar but with $x_{c2} = 1.0$. It is desired to reduce Equation (49) to two degrees-of-

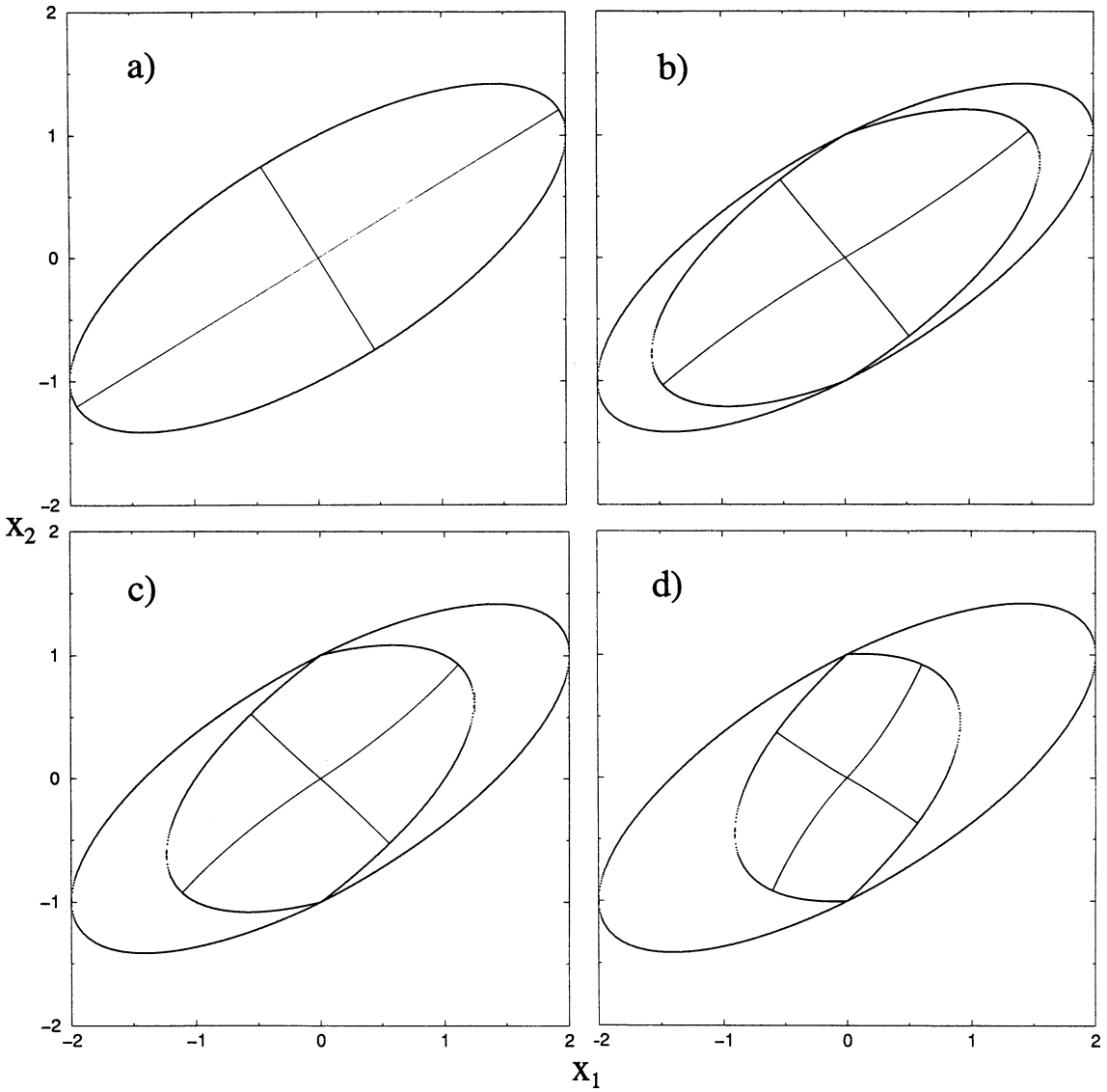

Fig. 15 Numerical simulations in configuration space of NNMs for the two-degree-of-freedom system with bang-bang nonlinearity with $\delta =$ (a) 0.0 (*linear*) (b) 0.25 (c) 0.5 (d) 0.875. The solid closed curves are the equipotential boundaries with and without the nonlinear spring

freedom in x_1 and x_2. First, the linear-based order reduction in Equations (4)–(7) is implemented by transforming Equation (49) via

$$\begin{bmatrix} x_1 \\ x_2 \\ x_3 \\ x_4 \end{bmatrix} = \begin{bmatrix} 1 & 0 \\ 0 & 1 \\ -1 & 1.8794 \\ -1 & 1.5321 \end{bmatrix} \begin{bmatrix} x_1 \\ x_2 \end{bmatrix} \tag{50}$$

Comparing with Equations (4) and (7), the matrix T (computed via Equation (5)) which defines the master–slave relation is seen in the lower half of the transformation matrix. This results in the reduced-order model

$$\begin{bmatrix} 3.0 & -3.412 \\ -3.412 & 6.879 \end{bmatrix} \begin{bmatrix} \ddot{x}_1 \\ \ddot{x}_2 \end{bmatrix} + \begin{bmatrix} 0.3 & -0.3412 \\ -0.3412 & 0.4241 \end{bmatrix} \begin{bmatrix} \dot{x}_1 \\ \dot{x}_2 \end{bmatrix} + \begin{bmatrix} 3.0 & -3.412 \\ -3.412 & 4.241 \end{bmatrix} \begin{bmatrix} x_1 \\ x_2 \end{bmatrix} + \begin{bmatrix} \beta_1 f_1(x_1) \\ \beta_2 f_2(x_2) \end{bmatrix} = 0 \tag{51}$$

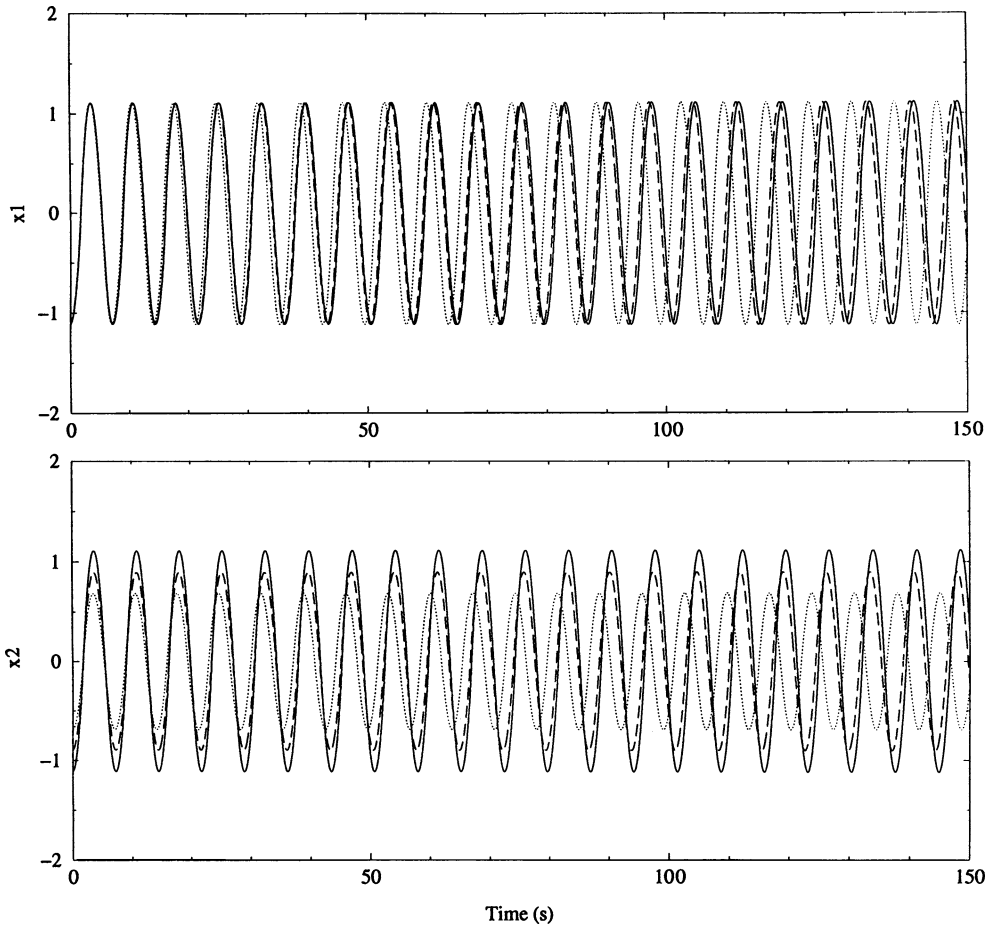

Fig. 16 Time series of reduced-order models of the 2-dof system with bang-bang nonlinearity in the first mode computed via the linear-based reduction (*dotted*), LELSM (*dashed*), and numerical simulation of the full model (*solid*) for $\delta = 0.5$

in which $\beta_1 = \beta_2 = 1$. As explained previously, the transformation of Equation (50) preserves the exact eigenstructure of the linear part of Equation (49). The linear-based reduced model can be improved upon by finding alternate values for β_1 and β_2 as shown below.

Depending on the values of x_{c1}, x_{c2}, and the initial total energy E, it is possible to have 1, 3, 5, 7 or 9 separate linear subregions. For the values of $x_{c1} = 1.25$, $x_{c2} = 1.0$ and initial energy $E = \frac{1}{2}\hat{x}^T K \hat{x} + \frac{1}{2}(\hat{x}_1 - x_{c1})^2 + \frac{1}{2}(\hat{x}_2 - x_{c2})^2 = 1$, there are initially 7 separate subregions with four distinct equipotential boundaries as shown in Fig. 17, which represents a projection of the potential hypersurface onto the $x_1 - x_2$ plane, although this will change as energy is dissipated from the system. Since the amplitudes of coordinates x_1 and x_2 depend on the mode for a given energy level, a separate $\rho_{k,i}$ must be computed for the ith mode for $k = 1, 2$. By first ignoring the damping and assuming the NNM manifold occurs on the first eigenvector of the stiffness matrix in Equation (49), the same procedure described in Section 6.2 for estimating the amplitudes can be applied and iterated to find that x_1 and x_2 intersect the equipotential $E = 1$ in region 4 at approximately 1.838 and 1.671, respectively, yielding $\rho_{1,1} = 0.680$ and $\rho_{2,1} = 0.598$ for the two deadzone nonlinearities in mode 1. Since only the first mode penetrates a boundary, the $\rho_{k,i}$ values for the other modes are unity.

The separate effects of the two deadzones on the lowest frequency are now found using LELSM by computing the lowest eigenfrequencies of the two undamped systems

$$\ddot{x} + \begin{bmatrix} k_{\text{eq1}} & -1 & 0 & 0 \\ -1 & 2 & -1 & 0 \\ 0 & -1 & 2 & -1 \\ 0 & 0 & -1 & 2 \end{bmatrix} x = 0 \tag{52}$$

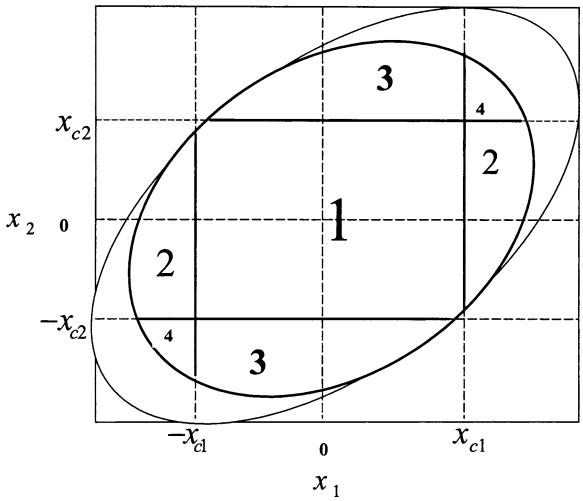

Fig. 17 Projection of the configuration space for the 4 degree-of-freedom system of Equation (49) with two deadzone nonlinearities onto the $x_1 - x_2$ plane. There are seven separate linear subregions with four distinct equipotential boundaries. (Not to scale.)

where $k_{\text{eq1}} = 1.202$ is obtained using $\rho_{1,1}$ and

$$\ddot{x} + \begin{bmatrix} 1 & -1 & 0 & 0 \\ -1 & k_{\text{eq2}} & -1 & 0 \\ 0 & -1 & 2 & -1 \\ 0 & 0 & -1 & 2 \end{bmatrix} x = 0 \tag{53}$$

where $k_{\text{eq2}} = 2.284$ is obtained using $\rho_{2,1}$. This yields $\Omega_{1,1} = 0.4466$ and $\Omega_{2,1} = 0.4570$ from Equations (52) and (53), respectively. Next, two single-degree-of-freedom reduced models of the undamped version of Equation (49)

$$\ddot{x}_i + 0.347^2 x_i + \tilde{\beta}_i \beta_i f_i(x_i) = 0 \tag{54}$$

$i = 1, 2$ are temporarily utilized (again considering the effects of the two deadzones separately) where 0.347 is the lowest frequency of the linear part of Equation (49) and $\tilde{\beta}_i \beta_i$ is the nonlinearity coefficient. Then, using $\Omega_{1,1}$, $\rho_{1,1}$, and $\alpha = \sqrt{2}$, Equation (34) can be solved numerically for $\tilde{\beta}_1 \beta_1 = 0.401$, while using $\Omega_{2,1}$ and $\rho_{2,1}$ yields $\tilde{\beta}_2 \beta_2 = 0.318$. Since the object is to find β_i, $\tilde{\beta}_i$ must first be determined. Now let Equation (54) represent the single-degree-of-freedom reduced models of the undamped version of the two-degree-of-freedom reduced model in Equation (51) (again considering the effects of the two deadzones separately). From this perspective, $\tilde{\beta}_i$ is the coefficient for the nonlinearity $\beta_i f_i(x_i)$. Since this nonlinearity is not completely known, however, PMM and LELSM cannot be used to find $\tilde{\beta}_i$. Instead, linear-based order reduction from Equation (51) to Equation (54) is now used to obtain $\tilde{\beta}_i = 0.431$ (using $\phi_1 = (1, 0.879)$) and $\tilde{\beta}_2 = 0.333$ (using $\phi_1 = (1.137, 1)$) from Equation (13). Now β_1 is calculated as $0.401/0.431 = 0.931$ and β_2 as $0.318/0.333 = 0.954$. The corresponding reduced model is then given by Equation (51) with these values of $\beta_{1,2}$.

In Fig. 18, the linear-based and improved reduced models in mode 1 (Equation (51)) are compared with simulation of Equation (49). Due to the damping, the amount of time that the system is in regions 2–4 of Fig. 17 decreases until the motion becomes purely linear (after about 95 s). It is seen that the time series of the improved reduced model obtained using LELSM is exactly in phase with that of the full model after the transition to linear vibration while that of the linear-based version has a constant lag in phase after this point. The difference in accuracy can also be observed in the undamped versions of Equations (49) and (51), for which the frequencies of the improved and linear-based reduced models are 0.5236 and 0.5285, respectively, while that of the full model is 0.5235. The initial displacement for the NNM was selected at the intersection of the first eigenvector of

$$K_{\text{eq}} = \begin{bmatrix} k_{\text{eq1}} & -1 & 0 & 0 \\ -1 & k_{\text{eq2}} & -1 & 0 \\ 0 & -1 & 2 & -1 \\ 0 & 0 & -1 & 2 \end{bmatrix} \tag{55}$$

(which approximates the dynamics only in the first mode) and the equipotential boundary for $E = 1$. It should be noted that, although this mode shape (1.0, 0.909, 0.811, 0.475) is an accurate linear approximation to the first NNM, it is not orthogonal to modes 2–4 which are extracted from the linear part of Equation (49) (because they do not penetrate a boundary). As was previously stated, this accurately reflects the fact that NNMs of nonsmooth systems are in general not orthogonal. An improved master–slave relation is found from this eigenvector as $x_3 = 0.811 x_1$ and $x_4 = 0.475 x_1$.

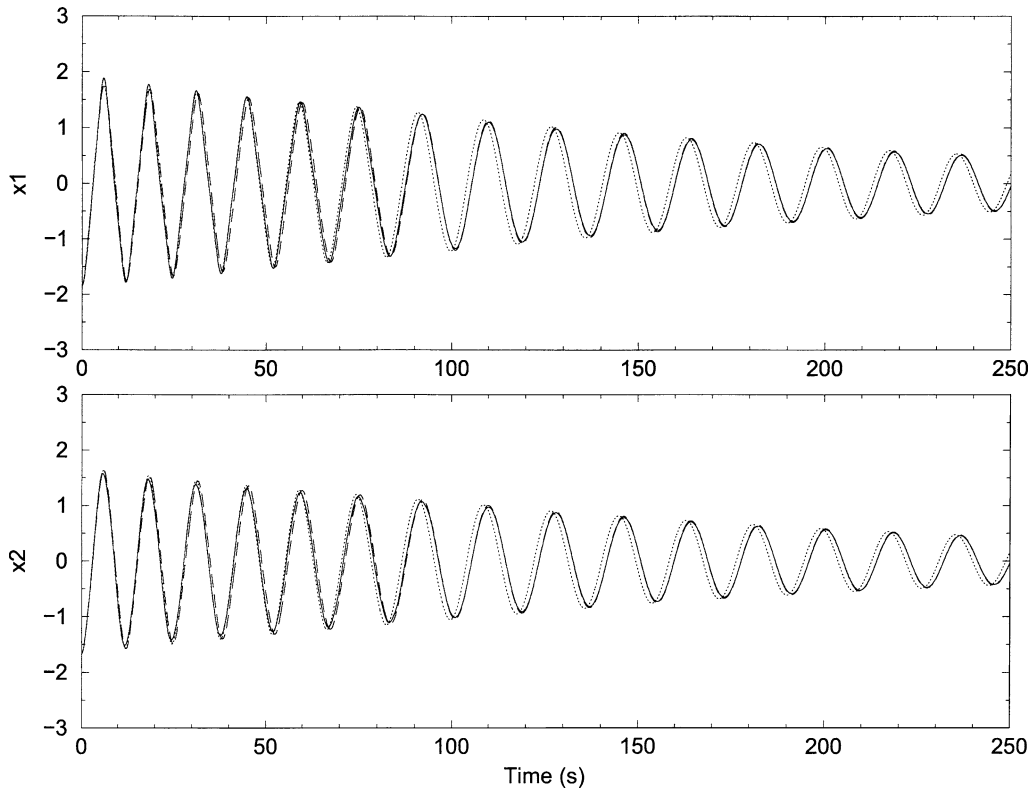

Fig. 18 Time series of reduced-order models of the damped four-degree-of-freedom system of Equation (49) with two deadzone nonlinearities in the first mode computed via the linear-based reduction (*dotted*), LELSM (*dashed*), and numerical simulation of the full model (*solid*) for $\alpha^2 = 2$, $x_{c1} = 1.25$, and $x_{c2} = 1.0$

8 Conclusions

A technique for order reduction of structural systems with piecewise linear static nonlinearities via NNM approximations has been presented. By employing PMM and LELSM, improved reduced-order models whose amplitude-dependent frequencies and mode shapes are better approximations to the exact NNM frequencies and mode shapes were obtained for bilinear clearance, deadzone, saturation, and bang-bang nonlinearities. Extension of the technique to multi-mode reduced-order models and multiple nonsmooth nonlinearities was also demonstrated with a four-degree-of-freedom example. In this case, the amplitudes of the masses were computed separately in each mode from a given total energy; consequently, it was seen that the piecewise nonlinearity is present in some modes while it does not influence others. The results obtained were compared with the exact NNM frequencies and the optimal linear mode shapes for the NNM manifolds obtained via least-squares regression from the direct numerical integration of the full models. It was seen that for bilinear clearance nonlinearity in the first mode PMM (which gives an amplitude-independent reduced model) was more accurate, while for the second mode and for all of the odd symmetric nonlinearities LELSM (which gives an amplitude-dependent reduced model) was more accurate. This can in part be explained by the different ways in which the methods approximate the NNM manifolds. Since PMM assumes that the dynamics occur on the piecewise union of the eigenvectors in the separate subregions joined at the boundary, there is discontinuity in this dynamic behavior whenever a boundary is not at the origin. In contrast, LELSM always approximates the dynamics on linear vectors which, like POMs, are accurate linear representations of the NNM manifold, although the complete set are not orthogonal in general.

We should point out that the success of these techniques depends on their ability to approximate a

nonlinear system with a linear one. Thus, the technique is designed for systems in which the linear part of the model dominates in the dynamics, with the same number of NNMs as degrees of freedom and the invariant manifold "straight enough" to be approximated by vectors. Hence, the best parameter choices to ensure convergence are those that result in weak nonlinearities (i.e. k_c small). However, the range of possible clearance (x_c) values is not limited by these methods. Although the techniques generally result in improved reduced models which are more accurate than the linear-based versions, possible sources are error include significant deviations of the NNM manifolds from the LELSM eigenvectors and the use of linear (albeit improved) master–slave coordinate relations. The inclusion of linear damping or forcing is done simply by ignoring their effects when calculating the improved nonlinearity coefficients. The advantages of the present technique include a reduced model which uses a subset of the original physical coordinates, contains the form of the nonsmooth nonlinearity of the full model, and can accommodate multiple nonsmooth nonlinearities with several surfaces of discontinuity through the use of an equivalent linear stiffness matrix. In this respect it is similar to the use of describing functions where individual nonlinearities are translated into equivalent linear gains. Since the method applies directly to structural vibrating systems in second order form, the need to use state-space coordinates is completely avoided, as is the process of calculating the exact NNM manifolds and corresponding dynamics. While the dependence of the LELSM-based reduced model on initial conditions (through the parameter ρ) may be an undesirable feature in some applications, the PMM-based reduced models avoid this since the improved nonlinear coefficient is computed from the two sets of linear eigenfrequencies in the two subregions. Finally, it was shown that numerical simulation of the full model is not required even for the amplitude-dependent LELSM-based method, since the intersection of the NNM manifold with the equipotential boundary for a given initial energy can be easily estimated.

Acknowledgment Financial support for this work was provided by the Air Force Office of Scientific Research under contract number F49620-01-1-0388 and the UAF Graduate School.

References

1. Gaul, L., Lenz, J.: Nonlinear dynamics of structures assembled by bolted joints. Acta Mechanica **125**, 169–181 (1997)
2. Choy, P.K., Padovan, J., Batur, C.: Rub interactions of flexible casing rotor systems. ASME J. Eng. Gas Turbines Power **111**, 652–658 (1989)
3. Flowers, G.T., Wu, F.: Disk shaft vibration induced by bearing clearance effects: analysis and experiments. ASME J. Vib. Acoust. 204–208 (1996)
4. Slotine, J.-J.E., Li, W.: Applied Nonlinear Control. Prentice Hall, New Jersey (1991)
5. Vakakis, A.F., Manevitch, L.I., Mikhlin, Y.V., Pilipchuk, V.N., Zevin, A.A.: Normal Modes and Localization in Nonlinear Systems. Wiley, New York (1996)
6. Zuo, L., Curnier, A.: Non-linear real and complex modes of conewise linear systems. J. Sound Vib. **174**, 289–313 (1994)
7. Chen, S.-L., Shaw, S.W.: Normal modes for piecewise linear vibratory systems. Nonlinear Dyn. **10**, 135–164 (1996)
8. Chati, M., Rand, R., Mukherjee, S.: Modal analysis of a cracked beam. J. Sound Vib. **207**, 249–270 (1997)
9. Butcher, E.A.: Clearance effects on bilinear normal mode frequencies. J. Sound Vib. **224**, 305–328 (1999)
10. Rhee, W., Burton, T.D.: Model reduction in structures with non-analytic nonlinearities. In: Proceedings of 8th Conference on Nonlinear Vibrations, Stability, and Dynamics of Structures, July 23–27, Virginia Polytechnic Institute and State University, Blacksburg, VA (2000)
11. Burton, T.D., Young, M.E.: Model reduction and nonlinear normal modes in structural dynamics. In: Proceedings of ASME IMECE, Chicago, IL, AMD Vol. 192, pp. 9–16 (1994)
12. Burton, T.D., Rhee, W.: On the reduction of nonlinear structural dynamic models. J. Vib. Control **6**, 531–556 (2000)
13. Jiang, D., Pierre, C., Shaw, S.: Large amplitude nonlinear normal modes of piecewise linear systems. J. Sound Vib. **272**, 869–891 (2004)
14. Shaw, S.W., Pierre, C.: Normal modes for non-linear vibratory systems. J. Sound Vib. **164**, 85–124 (1993)
15. Shaw, S.W., Pierre, C., Pesheck, E.: Modal analysis-based reduced-order models for nonlinear structures – an invariant manifold approach. Sound Vib. Digest **31**, 3–16 (1999)
16. Pesheck, E., Pierre, C., Shaw, S.: Modal reduction of a nonlinear rotating beam through nonlinear normal modes. ASME J. Vib. Acoust. **124**, 229–236 (2002)
17. Guyan, R.J.: Reduction of stiffness and mass matrices. AIAA J. **3**, 380 (1965)
18. Shaw, S.W., Holmes, P.J.: A periodically forced piecewise linear oscillator. J. Sound Vib. **90**, 129–155 (1983)
19. Nayfeh, A.H., Mook, D.T.: Nonlinear Oscillations. Wiley, New York (1979)
20. Feeny, L., Kappagantu, R.: On the physical interpretation of proper orthogonal modes in vibrations. J. Sound Vib. **211**, 607–616 (1998)
21. Kerschen, G., Golinval, J.-C., Vakakis, A.F., Bergman, L.A.: The method of proper orthogonal decomposition for dynamical characterization and order reduction of mechanical systems: an overview. Nonlinear Dyn. **41**, 147–169 (2005)